APS physics

CHORUS

This is the accepted manuscript made available via CHORUS. The article has been published as:

Isoscaling of heavy projectile residues and N/Z equilibration in peripheral heavy-ion collisions below the Fermi energy

G. A. Souliotis, P. N. Fountas, M. Veselsky, S. Galanopoulos, Z. Kohley, A. McIntosh, S. J. Yennello, and A. Bonasera

Phys. Rev. C **90**, 064612 — Published 15 December 2014

DOI: 10.1103/PhysRevC.90.064612

Isoscaling of heavy projectile residues and N/Z equilibration in peripheral heavy-ion collisions below the Fermi energy.

G. A. Souliotis[1,2,*] P. N. Fountas[1], M. Veselsky[3], S. Galanopoulos[2,†]
Z. Kohley[2,4,‡] A. McIntosh[2], S. J. Yennello[2,4], and A. Bonasera[2,5]
[1] *Laboratory of Physical Chemistry, Department of Chemistry, National and Kapodistrian University of Athens, Athens 15771, Greece*
[2] *Cyclotron Institute, Texas A&M University, College Station, Texas 77843, USA*
[3] *Institute of Physics, Slovak Academy of Sciences, Bratislava 84511, Slovakia*
[4] *Chemistry Department, Texas A&M University, College Station, TX 77843, USA and*
[5] *Laboratori Nazionali del Sud, INFN, via Santa Sofia 62, I-95123 Catania, Italy*
(Dated: November 25, 2014)

The isoscaling of heavy projectile residues from peripheral heavy-ion reactions at 15–25 MeV/nucleon is employed to obtain information on the process of N/Z equilibration. Recent mass spectrometric data of projectile residues from the reactions of ^{86}Kr (15 MeV/nucleon) with ^{64,58}Ni and ^{124,112}Sn were first analyzed. The isotopically resolved yield distributions of the fragments in the range Z=26–39 were employed for the isoscaling analysis. The yield ratios R_{21}(N,Z) of the fragments from each pair of systems exhibit isoscaling (i.e. an exponential dependence on the fragment neutron number N for each atomic number Z) with the isoscaling parameter α increasing with decreasing (or increasing) Z away from the projectile. This variation is related to the evolution toward N/Z equilibration with increasing energy dissipation estimated from the residue velocities. In parallel to the new heavy-residue isoscaling data of ^{86}Kr at 15 MeV/nucleon, our previous data at 25 MeV/nucleon for the reactions ^{86}Kr+^{124,112}Sn and ^{64}Ni+^{64,58}Ni, ^{64}Ni+^{124,112}Sn, as well as our data at 15 MeV/nucleon of the lighter system ^{40}Ar+^{64,58}Ni were analyzed in a similar way. Calculations with the stochastic nucleon-exchange model DIT (Deep Inelastic Transfer) and the microscopic many-body model CoMD (Constrained Molecular Dynamics) provided an overall fair description of data and valuable guidance for their interpretation. Interestingly, the data of the ^{86}Kr+Ni,Sn reactions at 15 MeV/nucleon show a retardation of the process of N/Z equilibration which, as suggested by the CoMD calculations, is indicative of the collective character of the process. This retardation is not present in the investigated systems at 25 MeV/nucleon (and the light ^{40}Ar+Ni systems at 15 MeV/nucleon), whose behavior is found to be consistent with stochastic nucleon exchange.

PACS numbers: 25.70.Mn,25.70.Lm,25.70.Pq
Keywords: Heavy-ion nuclear reactions, peripheral collisions, deep-inelastic transfer, isoscaling, N/Z equilibration, constrained molecular dynamics

I. INTRODUCTION

New frontiers in the study of the nuclear many-body problem open up with the availability of Rare Isotope Beams (RIB) worldwide. Among these, the investigation of very neutron-rich rare isotopes offers the possibility to follow the evolution of nuclear structure with increasing neutron-to-proton ratio (N/Z) [1–3], and to elucidate important nucleosynthesis processes [4, 5], such as the rapid neutron-capture process (r-process) [6, 7]. In parallel, reactions induced by isospin-asymmetric nuclei (either neutron-rich or neutron deficient) offer unique opportunities to explore the properties of the effective nucleon-nucleon interaction and, thus, shed light on the equation of state [8–13] of asymmertic nuclear matter, which, in turn plays a pivotal role in the physics of supernova [14–16] and neutron stars [17–19]. In reactions among isospin asymmetric nuclei, in particular, the N/Z degree of freedom and its equilibration may serve as valuable probes of the symmetry energy term of the nuclear equation of state [11–13, 20, 21].

Extensive work in deep-inelastic heavy-ion collisions at low energies (E/A<10 MeV, for a review see, e.g., [22, 23]) provided insight into the relevant reaction mechanisms [24–29]. At these energies, the collisions are of binary character involving a transient dinuclear complex. A fast redistribution of neutrons and protons takes place between the interacting projectile and target during the interaction time and is responsible for the process of N/Z (or isospin) equilibration. At medium energies, relevant work [30–35] indicated that essentially above the Fermi energy isospin equilibrium is not reached even for the most damped collisions. In these studies, isotopic or isobaric yield ratios of selected light or intermediate-mass fragments were used to probe isospin equilibration in semi-peripheral to near-central collisions. Insight into isospin equilibration has also been provided in re-

*Corresponding author. Email: soulioti@chem.uoa.gr
†Present address: Greek Army Academy, Department of Physical Sciences, Athens, Greece
‡Present address: National Superconducting Cyclotron Laboratory, Michigan State University, E. Lansing, MI, USA

cent studies of reconstructed quasiprojectiles undergoing multifragmentation following a deep-inelastic collision [36, 37].

In addition, recent work has focused on the investigation of the enhanced N/Z ratio of fragments emitted at midvelocity (commonly referred to as "neck" emission) [38–42]. Furthermore, detailed studies of the timescale of N/Z equilibration in a dinuclear complex consisting of the projectile and (part of) a low-density neck attached to it after a semiperipheral collision are presented in [43, 44].

From a theoretical point of view, a successful description of the features of the process of N/Z equilibration was obtained with phenomenological models based on stochastic nucleon exchange [24, 45–47]. More sophisticated microscopic approaches have also been adopted including semiclassical mean-field transport models of Boltzmann-type such as BUU (Boltzmann-Uehling-Ulenbeck) [9, 31, 48, 49], BNV (Boltzmann-Nordheim-Vlasov) [11, 50], SMF (Stochastic Mean Field) [11, 51] and the fully quantal TDHF (time-dependent Hartree-Fock) approach [52–54]. Furthermore, N-body approaches of Quantum Molecular Dynamics (QMD) type [55] have been applied such as the Constrained Molecular Dynamics (CoMD) model [56, 57] employed in this work.

Whereas a number of features of the process of N/Z equilibration at energies above the Coulomb barrier were successfully described via stochastic nucleon exchange, it has been shown in transport calculations (e.g. [58–60] and ref. therein) that the process has a collective character resembling a large amplitude dipole motion. This collective mode has been termed as the dynamical dipole mode and corresponds to an isovector giant dipole resonance (GDR) motion in the dinuclear system formed by the projectile and the target during their interaction time. Recent systematic experiments have confirmed the development of this mode via the observation of extra γ-ray yields in the energy region at and below the well known statistical GDR ([61, 62] and ref. therein).

At higher energies, toward the Fermi energy, mainly due to the increasing importance of nucleon-nucleon collisions, it is expected that the collective character of the process will give place to direct isospin transport, essentially due to stochastic nucleon exchange. In a binary reaction scenario between isospin asymmetric nuclei, the neutron and proton currents $\mathbf{j}_n$ and $\mathbf{j}_p$ can be expressed as linear combinations of the gradients of the local density $\rho = \rho_n + \rho_p$ and isospin $I = \frac{\rho_n - \rho_p}{\rho}$:

$$\mathbf{j}_n = D_n^\rho \nabla\rho - D_n^I \nabla I \tag{1}$$

$$\mathbf{j}_p = D_p^\rho \nabla\rho - D_p^I \nabla I \tag{2}$$

In these expressions, D_n^ρ, D_p^ρ are the neutron, proton transport coefficients due to density gradients (mass-transport coefficients) and D_n^I, D_p^I are the neutron, proton transport coefficients due to isospin gradients. Expressions for these transport coefficients are given in [50]. Taking the difference of these equations, we can obtain the isospin (neutron-excess) current $\mathbf{j}_{np} = \mathbf{j}_n - \mathbf{j}_p$

$$\mathbf{j}_{np} = \mathbf{j}_n - \mathbf{j}_p = (D_n^\rho - D_p^\rho)\nabla\rho - (D_n^I - D_p^I)\nabla I \tag{3}$$

The differences of the corresponding diffusion coefficients [50] have the following simple dependences:

$$D_n^\rho - D_p^\rho \propto 4\, I \frac{\partial S_{sym}(\rho)}{\partial\rho} \tag{4}$$

$$D_n^I - D_p^I \propto 4\,\rho\, S_{sym}(\rho) \tag{5}$$

where $S_{sym}(\rho)$ represents the density dependent nuclear symmetry energy. According to these expressions that are also presented and discussed in other references (e.g. [9, 20]), we can clearly see that isospin transport may be due to density gradients (referred to as isospin drift or isospin migration) and/or isospin gradients (referred to as isospin diffusion). In the first case the transport is proportional to the slope of the symmetry energy $S_{sym}(\rho)$ (symmetry pressure), whereas in the second case the transport is proportional to the absolute value of $S_{sym}(\rho)$.

In a (nearly) uniform region of neutrons and protons ($\rho \sim$ const.), the isospin current can be written as:

$$\mathbf{j}_{np} = -(D_n^I - D_p^I)\nabla I \tag{6}$$

Employing the continuity equation for the isospin I,

$$\nabla \bullet \mathbf{j}_{np} + \frac{\partial I}{\partial t} = 0$$

we obtain a diffusion equation (Fick's law) for I:

$$\frac{\partial I}{\partial t} = (D_n^I - D_p^I)\nabla^2 I \tag{7}$$

Expoiting the linearity of this differential equation, and applying it (under identical conditions), first to a neutron-rich system with isospin I_2 and, second, to a neutron-deficient system with isospin I_1, we get:

$$\frac{\partial(\Delta I)}{\partial t} = (D_n^I - D_p^I)\nabla^2(\Delta I) \tag{8}$$

where $\Delta I = I_2 - I_1$ is the isospin difference between the two systems to be compared, as usually employed in an isoscaling analysis. The above equations indicate that the rate of isospin diffusion is proportional to the difference $D_n^I - D_p^I$, and thus (according to Eq. 5) proportional to the strength of the symmetry energy $S_{sym}(\rho)$ at the corresponding density. Equations 7 and 8 will be useful in the interpretation of the results of the present study (Section V-C).

Focusing our attention on the N/Z equilibration between a projectile and a target in a binary collision, it would be of interest to probe experimentally the evolution toward N/Z equilibrium with respect to the degree of

energy dissipation from quasi-elastic to the most damped collisions. In such efforts, the properties of heavy residues appear to be very useful. As well known, in collisions at low and medium energies, a large fraction of the reaction cross section corresponds to the production of heavy residues, i.e., large surviving remnants of the projectile (or target) after evaporation of neutrons, protons or light charged particles [63]. Due to the binary character of the collision, the velocities of the residues are strongly correlated to their mass, and can thus provide information on the energy dissipation and, furthermore, on the excitation energy imparted into the collision partners.

The N/Z of the residue is reminiscent of the N/Z of the corresponding hot primary fragment (quasiprojectile, QP), but the former is affected by the evaporation process. Efforts to reconstruct the quasiprojectile [25, 26] based on evaporation codes provided some information on the process of N/Z equilibration as a function of energy dissipation and thus, the interaction time. In our previous work at 25 MeV/nucleon [64], using an isoscaling approach, we obtained information on the process of N/Z equilibration for the reaction ^{86}Kr + ^{124,112}Sn as a function of the excitation energy of the quasiprojectile.

In the present study, we will describe the results of heavy residue isoscaling at 15–25 MeV/nucleon and extend our previous approach [64] to follow the process of N/Z equilibration with respect to the degree of the energy dissipation. Our analysis employs the yield ratios of isotopically resolved heavy projectile residues obtained from a pair of isospin-asymmetric reactions in conjunction with high-resolution measurement of the residue velocities. This article is organized as follows. In section II, a concise description of the recent experimental measurements of heavy projectile residues from the reactions of ^{86}Kr (15 MeV/nucleon) with ^{64}Ni,^{58}Ni and ^{124}Sn,^{112}Sn targets is given. In section III, the analysis of residue yield ratios and the procedure to extract information about the process of N/Z equilibration with respect to energy dissipation are described. In Section IV, a brief description of the DIT and CoMD models is given. In Section V, a comparison of the calculations with the experimental data is given. Along with the isoscaling data of ^{86}Kr at 15 MeV/nucleon, our previous 25 MeV/nucleon data for the reactions ^{86}Kr+^{124,112}Sn [64] and ^{64}Ni+^{64,58}Ni,^{124,112}Sn [65], as well as, our 15 MeV/nucleon data for ^{40}Ar+^{64,58}Ni [66] are presented and compared with the DIT and CoMD calculations. Finally, in Section VI a discussion is presented, followed by a summary in Section VII.

II. EXPERIMENTAL PROCEDURE

The experimental data of the present work at 15 MeV/nucleon and the analysis procedures are described in detail in our recent article [67] in which a systematic study of the production cross sections of heavy projectile fragments from 15 MeV/nucleon ^{86}Kr-induced reactions on ^{64,58}Ni and ^{124,112}Sn is reported. Herein we present a subsequent analysis of the same yield data with the aim of obtaining information on the isoscaling behavior of the heavy residues and the process of N/Z equilibration. For completeness, a short description of the experimental measurements follows. The measurements were performed at the Cyclotron Institute of Texas A&M University. A 15 MeV/nucleon ^{86}Kr beam of ∼1–5 pnA (∼0.6–3×10^{10} particles/s) from the K500 superconducting cyclotron interacted with isotopically enriched ^{64}Ni,^{58}Ni and ^{124}Sn,^{112}Sn targets. Projectile residues were analyzed with the MARS recoil separator [68]. In order to cover the appropriate angular range for the reactions studied, the experiment was divided in two parts: In the first part ("4^o data"), the primary beam struck the target at an angle of 4.0^o relative to the optical axis of the spectrometer and, fragments were accepted in the polar angular range of 2.2^o–5.8^o. In the second part ("7^o data"), the beam hit the target at an angle of 7.4^o and the fragments were collected in the polar angular range of 5.6^o–9.2^o.

For the present study, we will employ the 4^o data for the 15 MeV/nucleon ^{86}Kr+^{64,58}Ni reactions that have a grazing angle of 6.0^o [69]. Moreover, we will use the 7^o data of the 15 MeV/nucleon ^{86}Kr+^{124,112}Sn reactions whose grazing angle is 9.0^o. Thus, for each reaction pair studied, the angular range in which the heavy residues are obtained lies inside the grazing angle of the corresponding system. Under these conditions, heavy residues from a wide range of impact parameters are collected, from very peripheral to semiperipheral collisions.

At the focal plane of MARS, the fragments were collected in a 5cm×5cm ΔE–E Si detector telescope. Time-of-flight was measured between two PPACs (parallel plate avalanche counters) placed at the MARS dispersive image and at the focal plane, respectively, separated by a distance of 13.2 m. The horizontal position provided by the first PPAC and the field measurement of the MARS first dipole magnet were used to determine the magnetic rigidity $B\rho$ of the fragments. The reaction products were characterized event-by-event using energy-loss, residual energy, time-of-flight, and $B\rho$. These quantities were calibrated with a low intensity ^{86}Kr beam and other beams at 15 MeV/nucleon. With the procedures described in Ref. [67, 70], the atomic number Z, the ionic charge q, the mass number A and the velocity of the fragments were obtained with high resolution. The resolutions of Z, q, A and velocity were 0.5, 0.4, 0.6 units and 0.3%, respectively, for near projectile residues. Summation over the ionic charge states provided the yield distributions with respect to Z, A and velocity from which the distributions employed in this work were obtained.

We note that the measurements were performed in the magnetic rigidity range of 1.1–2.0 T m (by superposition of successive magnetic settings of the separator) and in the angular ranges of 2.2^o–5.8^o (4^o data) and 5.6^o–9.2^o (7^o data). As mentioned above, these angular ranges lie inside the grazing angles of the Kr+Ni and Kr+Sn sys-

tems, respectively, at 15 MeV/nucleon. The Bρ range and the angular ranges enabled efficient collection of heavy projectile residues produced in a large range of energy damping, from quasielastic to deep-inelastic collisions. Further details of the analysis procedure can be found in [67, 70] and in our previous work with heavier beams ([71] and references therein). The yield distributions, summed over velocities, were used to obtain the yield ratios $R_{21}(N,Z) = Y_2(N,Z)/Y_1(N,Z)$ employed in the present isoscaling studies.

III. EXPERIMENTAL RESULTS

A. Isoscaling behavior of heavy projectile residues

We will first examine the isoscaling properties of the heavy projectile residue yields from the reactions of ^{86}Kr (15 MeV/nucleon) with ^{64,58}Ni and ^{124,112}Sn. We briefly note that the ratio $R_{21} = Y_2(N,Z)/Y_1(N,Z)$ of the yields of a given fragment (N,Z) from two sources with similar excitation energies and similar masses, which differ only in N/Z, follows the isoscaling relation [72–74], namely, an exponential dependence with respect to N and Z of the form:

$$R_{21}(N,Z) = Y_2(N,Z)/Y_1(N,Z) = C\exp(\alpha N + \beta Z) \quad (9)$$

The scaling parameters α and β, within a grand canonical description, can be expressed as $\alpha = \Delta\mu_n/T$ and $\beta = \Delta\mu_p/T$, with $\Delta\mu_n$ and $\Delta\mu_p$ being the differences in the neutron and the proton chemical potentials and T the temperature of the fragmenting systems [72]. C is an overall normalization constant. The isoscaling relation has been obtained in many different types of reactions such as multifragmentation [72, 73], light ion-induced fragmentation or spallation [74], deep-inelastic reactions [65, 75, 76], and fission [77] (for a recent review, see, e.g. [78]).

For the present data, we obtained the yield ratio $R_{21}(N,Z)$ using the usual convention that index 2 refers to the more neutron-rich system and index 1 to the less neutron-rich one. Figs. 1a, 1b show the isotopic yield ratios R_{21}(N,Z) as a function of fragment neutron number N for several isotopes in the range Z=26–39 for the two reaction pairs ^{86}Kr (15 MeV/nucleon) + ^{64,58}Ni and ^{86}Kr (15 MeV/nucleon) + ^{124,112}Sn, respectively. Exponential functions of the form $Cexp(\alpha N)$ were fitted to the data and are shown in Figs. 1a, 1b for the selected isotopes. (The undulatory variation of the data points for each Z especially those close to the projectile is commented in Section VI). In Fig. 2, we present the extracted logarithmic slope parameter α (referred to as the isoscaling parameter) as a function of Z for the two reaction pairs: ^{86}Kr+Ni (open symbols) and ^{86}Kr+Sn (closed symbols). We note that for Z=36 we could not obtain an isoscaling line, due to the presence of intense elastic scattering, thus the corresponding isoscaling parameter value is absent from Fig. 2. We observe that the isoscaling parameter α increases gradually for fragments with Z further away from that of the projectile. This variation, observed in our previous work at 25 MeV/nucleon [64, 75] has been attributed to the degree of N/Z equilibration as a function of dissipation and thus the interaction time (see discussion below).

B. Determination of dissipation and excitation energy

After presenting the isoscaling behavior, we will examine the velocity characteristics of the observed heavy residues. We note that reactions between heavy ions around and below the Fermi energy [63] proceed via a deep-inelastic transfer mechanism involving substantial nucleon exchange [36, 79–81]. This mechanism is responsible for energy dissipation and the ensuing creation of highly excited primary fragments. In a binary reaction scenario, two primary fragments are produced: the quasiprojectile (QP) and the quasitarget (QT) that deexcite to produce the observed fragments. To obtain information on the amount of energy dissipation from the present reactions, we will examine the correlation of the measured velocity with the atomic number Z of the heavy projectile residues. In Fig. 3a we present the average velocities of the observed fragments as a function of Z. Open symbols correspond to the reaction ^{86}Kr+^{64}Ni and closed symbols to ^{86}Kr+^{124}Sn. (The velocity data from the reactions with the neutron-deficient targets are essentially similar to those presented in this figure for the neutron-rich targets and are omitted). The horizontal dashed line corresponds to the velocity of the projectile. In this figure, we observe that for fragments close to the projectile, the velocities are slightly below that of the projectile, corresponding to peripheral, low-dissipation events. A decrease of velocity with decreasing Z (as well as with increasing Z, for the trans-projectile residues Z=37–39) is observed, indicating progressively higher energy dissipation and, thus, higher excitation energies imparted to the reaction partners.

For both reactions Kr+Ni and Kr+Sn (Fig. 3a), the descending velocity–Z correlation continues down to Z$\sim$26. The appearance of a minimum velocity for Z$\sim$26-27, clearly discernible for the Kr+Ni reaction, can be understood as follows: Fragments with Z near the projectile down to Z$\sim$27 originate from evaporative type of deexcitation which does not modify, on average, the emission direction of the residues. Consequently, the average residue velocities can provide information on the energy dissipation. We note that our previous data on Kr+Sn at 25 MeV/nucleon [64] indicated similar behavior (see also Fig. 4 below). For those data, fragments with lower Z were also observed and their velocities appeared to increase with decreasing Z. As we noted in [64], residues with lower Z may arise from primary fragments undergoing cluster emission and/or multifragmentation and, in

such cases, the average velocity of the inclusively measured fragments is not monotonically correlated with the degree of energy dissipation.

For the present Kr+Ni, Kr+Sn reactions at 15 MeV/nucleon, for each heavy-residue Z, we employed the average velocity (Fig. 3a) and, furthermore, we applied two-body kinematics, to obtain an estimate of the total kinetic energy loss (TKEL) and the total excitation energy corresponding to this Z. The following procedure was applied: for each residue Z, the average mass $\langle A \rangle$ was obtained. For this residue, a number of nucleons $\Delta A = \Delta Z + \Delta N$ was assumed to be evaporated from the primary residue (quasiprojecile) to give the observed mass $\langle A \rangle$ and charge Z. For this evaporated mass, the number of neutrons and protons was chosen at random with a mean neutron-to-proton ratio of 3. (Variation of the neutron-to-proton ratio in the range 2–5 lead to insignificant variation of the kinematical results.) Using the quasiprojectile mass $A_{QP} = \langle A \rangle + \Delta A$ and charge $Z_{QP} = Z + \Delta Z$ and assuming binary kinematics, the binary reaction Q-value was obtained, which essentially gives the energy dissipation (total kinetic energy loss, TKEL): $TKEL = -Q$. Employing standard mass tables [82] for the ground-state to ground-state Q-value, Q_{gg}, the excitation energy for the binary system was obtained $E^* = Q_{gg} - Q$.

Regarding the sharing of the total excitation energy E^* between the quasiprojectile and the quasitarget, a reasonable assumption for peripheral collisions is equal division [36, 83, 84] at relatively low kinetic energy losses. This assumption was employed in our previous analysis of heavy-residue isoscaling data [64]. In the present work, we use a more appropriate prescription in agreement with the experimentally observed transition of the excitation energy sharing from the equal division limit (at low TKEL) toward the thermal limit near the maximum of the kinetic energy loss TKEL_{max}. Specifically, we estimated the excitation energy E^*_{QP} of the quasiprojectile assuming a linear evolution, with respect to $\mathrm{TKEL}/\mathrm{TKEL}_{max}$, from the equal division limit $E^*_{QP} = E^*/2$ to the thermal equilibrium limit $E^*_{QP} = E^* A_{QP}/(A_{QP} + A_{QT})$ (where A_{QT} is the quasitarget mass).

In our procedure, the excitation energy E^*_{QP} was assumed to be removed from the quasiprojectile by the sequential emission of the ΔA nucleons. At each evaporation stage, the evaporated nucleon carried away an amount of excitation energy equal to $E_{ev} = B_n + 2T$, where B_n is the average binding energy per nucleon (taken as $B_n = 8$ MeV) and T the temperature of the quasiprojectile (calculated with the Fermi-gas relation, see also below) at the corresponding evaporation step. With the above procedure, the value of ΔA was determined iteratively (starting from $\Delta A = 0$) in such a way that the number of ΔA nucleons was appropriate to remove the excitation energy E^*_{QP} from the assumed quasiprojectile. As an example, for Z=32 the average observed mass is $\langle A \rangle = 72$. The kinematical reconstruction gives $Z_{QP} = 34$ and $A_{QP} = 80$, TKEL = 225 MeV and $E^*_{QP} = 116$ MeV.

In Fig. 3b, the values of the TKEL as a function of residue Z from the 15 MeV/nucleon Kr+Ni and Kr+Sn data are presented (open points for Kr+Ni, closed points for Kr+Sn). The arrows correspond to the maximum TKEL (lower arrow for Kr+Ni, upper arrow for Kr+Sn). The excitation energy per nucleon of the quasiprojectiles as a function of Z is given in Fig. 3c (open points for Kr+Ni, closed points for Kr+Sn). We note that in Fig. 3, the errorbars in the average velocities are statistical (and very small owing to the good determination of the velocity of the residues), the errorbars ($\sim 5\%$) in Figs 3b and 3c are indicative of the uncertainties in the involved procedure of TKEL reconstruction. We note that for the subsequent discusion, the excitation energy will refer only to the quasiprojectile, so we will omit the designation "QP", and simply present as E^*/A the excitation energy per nucleon of the quasiprojectile. We observe that as we move from Z$\sim$36 down to Z$\sim$26, the corresponding values of E^*/A of the quasiprojectiles increase up to 2.0–2.5 MeV/nucleon (values approaching the nuclear multifragmentation threshold of $\sim$3 MeV/nucleon). A closer examination of the lower Z points, Z=26–28, shows that for the Kr+Ni system, E^*/A approaches 2.5 MeV/nucleon and the velocity appears to be nearly constant (Fig. 3a), possibly due to the onset of cluster emission or multifragmentation. For Kr+Sn, E^*/A is about 2.0 MeV/nucleon and the velocity continues to decrease monotonically, possilby due to the persistence of evaporative deexcitation (see relevant discussion above).

For completeness of our study and comparison of the present 15 MeV/nucleon data with our previous isoscaling data at 25 MeV/nucleon [64], we reanalysed the 25 MeV/nucleon data with exactly the same procedure applied to the 15 MeV/nucleon data of the present work. (We mention that these 25 MeV/nucleon data on ^{86}Kr+^{124,112}Sn were obtained with the MARS recoil separator in the angular range $\Delta\theta = 2.7^o$–5.4^o which lies inside the grazing angle of 6.5^o of the system Kr+Sn at this energy.) For this purpose, we first show in Fig. 4a the data of the isoscaling parameter α for the ^{86}Kr(25 MeV/nucleon)+^{124,112}Sn reactions presented in [64]. For this reaction we show projectile residues in the range Z=26–36 (trans-projectile residues were not collected in that experiment). In Fig. 4b we present the average velocity vs Z correlation. Conclusions similar to the study at 15 MeV/nucleon pertain (see also [64]). Following the procedures described above for the 15 MeV/nucleon data, we obtained the TKEL (Fig. 4c) and the quasiprojectile E^*/A (Fig. 4d) as a function of residue Z. We wish to comment on the lower Z values Z=26–28. For Z=28 and Z=26, the values of E^*/A are $\sim$3.4 and 3.8 MeV/nucleon, respectively, having already exceeded the nuclear multifragmentation threshold. Thus, for these isotopes the inclusively measured average velocity may not be strongly correlated with energy dissipation. (The average residue velocity appears to increase with decreas-

ing Z due to kinematical selection, see also [64].) We also note that for the 25 MeV/nucleon Kr+Sn system (with a maximum TKEL of 1040 MeV), we observe, as expected, much larger TKEL for each residue Z with respect to the values of the same system at 15 MeV/nucleon.

For both the 15 MeV/nucleon data of the present work and the 25 MeV/nucleon data of Kr+Sn [64], the temperatures of the quasiprojectiles were obtained from the extracted E*/A values using the Fermi-gas relationship $E^* = \frac{A}{K}T^2$, with T the tempretature and K the inverse level density parameter taken to be K=12 [85, 86].

C. Information on N/Z equilibration

In the following discussion, we will describe the procedure to obtain information on the process of N/Z equilibration employing the extracted isoscaling parameters, the excitation energy and temperature of the quasiprojectiles and the degree of dissipation expressed by the TKEL. As in our previous work at 25 MeV/nucleon [64], we will use the standard isoscaling formula:

$$\alpha = 4\,\frac{C_{sym}}{T}\Delta_{Z/A} \tag{10}$$

with

$$\Delta_{Z/A} = (\frac{Z_1}{A_1})^2 - (\frac{Z_2}{A_2})^2 \tag{11}$$

where α is the isoscaling parameter, C_{sym} the coefficient of the symmetry energy term of the nuclear binding energy; Z_1, A_1 and Z_2, A_2 refer to the fragmenting quasiprojectiles from reactions 1 and 2, respectively and T is their common temperature. We note that Eq. 10 has been obtained in a variety of theoretical approaches including the grand canonical limit of the statistical multifragmentation model (SMM) [74], the expanding–emitting source (EES) model [73] and mean-field models [87]. It has been primarily used to obtain C_{sym} or C_{sym}/T from the isoscaling parameter α at known (or measured) values of $\Delta_{Z/A}$ (see e.g. [88–90] and references therein).

For ease of interpretation in the following discussion, we will express the quantity $\Delta_{Z/A}$ with respect to N/Z of the quasiprojectiles and use it in Eq. 10 to obtain the expression [64]:

$$\alpha = 8\,\frac{C_{sym}}{T}(\frac{Z}{A})^3_{ave}\,\Delta_{N/Z} \tag{12}$$

with

$$\Delta_{N/Z} = \frac{N_2}{Z_2} - \frac{N_1}{Z_1} \tag{13}$$

where $(Z/A)_{ave}$ is the average Z/A of the quasiprojectiles taken to be the average Z/A of the two composite systems. In the following discussion, the quasiprojectile N/Z difference $\Delta_{N/Z}$ will be simply referred to as Δ.

In our approach, for each residue Z we use the isoscaling parameter α, the temperature T and the typical value C_{sym}=23 MeV for normal-density nuclei to obtain the quantity Δ via Eq. 12. Furthermore, since each Z has been correlated to a given average energy dissipation (Figs. 3b and 4c), we finally obtain a correlation of Δ with respect to TKEL. These correlations are shown in Figs. 6b and 7b for the 15 MeV/nucleon ^{86}Kr+^{64,58}Ni and ^{86}Kr+^{124,112}Sn data, respectively and in Fig. 8b for the 25 MeV/nucleon ^{86}Kr+^{124,112}Sn data. For the same systems, the absolute values of N/Z are presented in Figs. 6a, 7a and 8a as a function of TKEL for the neutron-rich systems (upper curves) and the neutron-deficient systems (lower curves) calculated with the codes DIT (dashed lines) and CoMD (solid and dotted lines). The description of the models and calculations is given in Section IV, along with a discussion of the correlation of TKEL with the interaction time (Fig. 5). In Figs 6a, 7a and 8a, the dashed horizontal line corresponds to the N/Z of the ^{86}Kr projectile, whereas the upper and lower horizontal solid lines give the N/Z of the quasiprojectiles coming from the neutron-rich and the neutron-deficient systems, respectively, assuming complete N/Z equilibration. We point out that the isoscaling approach cannot provide data on the absolute values of the N/Z of the quasiprojectiles, thus, of course, no experimental points are shown in Figs. 6a, 7a and 8a. Only the differences in the N/Z of the quasiprojectiles coming from the neutron-rich and the neutron-deficient systems can be obtained experimentally as explained before and are shown by the points in Figs. 6b, 7b and 8b. In these figures, the lines represent the differences Δ of the theoretical N/Z values calculated, as stated above, with the DIT and the CoMD models. The horizontal full line gives the N/Z difference of fully N/Z equilibrated quasiprojectiles.

The correlations presented in Figs. 6, 7 and 8 show the evolution of the N/Z equilibration process in the present isospin-asymmetric collisions. Qualitatively, the monotonic increase of Δ with energy dissipation can be understood as a result of nucleon transport. Fragments close to the projectile are produced in very peripheral collisions in which a small number of nucleons is exchanged and thus, the N/Z difference of the quasiprojectiles from the neutron-rich and the neutron-deficient systems is small. Fragments progressively further from the projectile originate from collisions with larger projectile–target overlap in which a large number of nucleons is exchanged and thus a larger amount of energy is dissipated. Thus, the N/Z difference of these quasiprojectiles is progressively larger, eventually approaching the N/Z difference corresponding to complete isospin equilibration.

Looking at the data, for the 15 MeV/nucleon ^{86}Kr+^{64,58}Ni (Fig. 6b) and ^{86}Kr+^{124,112}Sn (Fig. 7b), the experimental values of Δ increase monotonically with increasing TKEL, from small values indicative of peripheral collisions and short interaction times toward values corresponding to full N/Z equilibration near the maximum of the TKEL. For the 25 MeV/nucleon ^{86}Kr+^{124,112}Sn

data (Fig. 8b), the correlation of the experimental values of Δ vs TKEL shows an analogous behavior. However, for these data, due to the onset of heavy-cluster emission and/or multifragmentation, the reconstructed TKEL for Z=28 and below may be lower than the actual value (see Fig. 4). The three rightmost points of Fig. 8b are thus at lower TKEL than they should be. Kinematical reconstruction of the quasiprojectiles corresponding to such events is necessary to precisely determine these larger TKEL and the corresponding excitation energies (see, e.g. [88, 89, 91]).

IV. DESCRIPTION OF THE THEORETICAL MODELS

As we already stated, we used two models to describe the dynamical stage of the reactions and the process of N/Z equilibration with respect to energy dissipation. The first model is the phenomenological deep-inelastic transfer (DIT) model of Tassan-Got [47, 92] which simulates stochastic nucleon exchange in a Monte Carlo fashion. In this model, the projectile and the target, assumed to be spherical, approach each other along Coulomb trajectories until they are within the range of the nuclear interaction. At this point the system is represented as two Fermi gases in contact. A window opens in the internuclear potential and stochastic transfer of nucleons may occur. The direction and type of transfer are decided by random drawing based on transfer probabilities. The transfer probabilities are calculated via a phase-space integral that accounts for Pauli blocking and involves a phase-space flux term, the barrier penetrability and the occupation probabilities. The nucleon transfer produces a variation in mass, charge, excitation energy and spin of the interacting nuclei. After the interaction, the primary projectile-like fragment (quasiprojectile) and target-like fragment (quasitarget) are excited and follow Coulomb trajectories. We point out that in DIT, the exchange of nucleons is assumed to be the only source of energy dissipation. Nucleon-nucleon collisions (mostly blocked by the Pauli principle for lower energy collisions) are not explicitly taken into account in the model. The calculations are performed for a wide range of impact parameters from very peripheral to semiperipheral collisions. The DIT model has been recently applied in a variety of studies at and below the Fermi energy (e.g. [36, 37, 64, 70, 93, 94]). In addition, the DIT code was employed to describe lower energy data [95]. In that study, a modification of the nuclear profiles was necessary implying an extended neck between the projectile and the target during their interaction time. In the present calculations, the DIT code with its standard parameters was employed.

The second model we employed is the microscopic Constrained Molecular Dynamics (CoMD) model designed for reactions near and below the Fermi energy [56, 57]. Following the general approach of Quantum Molecular Dynamics (QMD) models [55], in the CoMD code nucleons are described as localized Gaussian wave packets. The wave function of the N-body nuclear system is assumed to be the product of these single-particle wave functions. With the Gaussian description, the N-body time-dependent Schödinger equation leads to (classical) Hamilton's equations of motion for the centroids of the nucleon wavepackets. The potential part of the Hamiltonian consists of a Skyrme-like effective interaction and a surface term. The isoscalar part of the effective interaction corresponds to a nuclear matter compressibility of K=200 (soft EOS) or K=380 (stiff EOS). For the isovector part, several forms of the density dependence of the nucleon-nucleon symmetry potential are implemented. Two of them will be used in the present work (Figs. 6–8, 10, 11 and 14): the "asy-stiff" potential [red (solid) line] and the "asy-soft" potential [blue (dotted) line] in the figures. These forms correspond to a dependence of the symmetry potential on the 1 and the 1/2 power of the density, respectively (see, also, [96] and references therein).

We note that in the CoMD model, while not explicitly implementing antisymmetrization of the N-body wavefunction, a constraint in the phase space occupation for each nucleon is imposed, effectively restoring the Pauli principle at each time step of the (classical) evolution of the system. This constraint restores in an approximate way the fermionic nature of the nucleon motion in the interacting nuclei. The short range (repulsive) nucleon-nucleon interactions are described as individual nucleon-nucleon collisions governed by the nucleon-nucleon scattering cross section, the available phase space and the Pauli principle, as usually implemented in transport codes. The latest CoMD version fully preserves the total angular momentum (along with linear momentum and energy) [57], features which are critical for the accurate description of observables from heavy-ion collisions.

In the present calculations, the CoMD code with its standard parameters was used. The soft density-dependent isoscalar potential was used (corresponding to a compressibility K=200 for symmetric nuclear matter) and the calculations were performed with either the asy-stiff or the asy-soft symmetry potential as mentioned above. The ground state configurations of the projectile and the target were obtained with a simulated annealing approach and were tested for stability for long times (1500–2000 fm/c). These configurations were used in the subsequent collision simulations. As with the DIT model, the calculations were performed in a wide range of impact parameters covering from peripheral to semiperipheral collisions. The calculations were stopped at t=300 fm/c and the observables of the produced quasiprojectiles were extracted and analyzed.

Before embarking on the discussion of the evolution of N/Z with respect to energy dissipation, we would like to investigate the relation between the projectile-target interaction time and the ensuing energy dissipation, as predicted by the DIT and CoMD model calculations. In Fig. 5, we show the correlation between the interaction

time t_{int} and the total kinetic energy loss, TKEL, as calculated by DIT (dashed lines) and CoMD (full lines) for reactions at 15 MeV/ nucleon (upper panel) and 25 MeV/ nucleon (lower panel). Apart from the ^{86}Kr reactions whose isoscaling data have already been presented, the reactions ^{40}Ar(15MeV/nucleon)+^{64,58}Ni and ^{64}Ni(25MeV/nucleon)+^{64,58}Ni,^{124,112}Sn are also shown for which the relevant isoscaling data will be discussed later. The arrows in Fig. 5 indicate the maximum expected TKEL for the respective reactions.

We observe that the DIT and CoMD predictions are rather similar for low TKEL, namely, below 100 MeV for the 15 MeV/nucleon reactions, and below 200 MeV for the 25 MeV/nucleon systems. For larger TKEL, there is a marked tendency of DIT to predict shorter t_{int} for given TKEL relative to CoMD, which becomes more pronounced at 25 MeV/nucleon. We note that similar results on the t_{int}–TKEL correlation for similar systems have been reported in Fig. 14 of [97] employing the nucleon-exchange model of [45] and the BNV transport model of [98]. The calculated t_{int}–TKEL correlations of Fig. 5 will be useful for our subsequent discussion in order to infer the interaction time (not a measured quantity in the experiments of this work) for given energy dissipation (a measured quantity, as discussed before).

Concluding this section on the description of the theoretical models, we wish to comment further on their physical basis. We remind that the DIT model is a phenomenological nucleon-exchange model with empirical parameters carefully chosen to describe peripheral reactions near the Fermi energy. On the other hand, the CoMD model is a fully microscopic (albeit semiclassical) model of the collisions employing empirical interactions among the nucleons that have been adjusted to describe the known static properties of nuclei (i.e., radii, masses, etc.) [56]. As such, the code has essentially no adjustable parameters that depend on the dynamics to be described. Furthermore, the CoMD model, at variance with mean-field models, naturally takes into account nucleon-nucleon correlations that are of vital importance for the description of observables involving fluctuations, as for example the nucleon transport in peripheral collisions as in the present work. (We remind that in mean-field transport models, effects beyond the mean field are simulated via nucleon-nucleon collisions, as well as fluctuations of the mean field [51, 53].) For these reasons, the CoMD predictions are especially valuable for the interpretation of the results of the present study. Moreover, the CoMD may be trusted when applied to regions where no experimental data are yet available, i.e., in reactions with rare isotope beams.

V. COMPARISONS

A. Confrontation of model calculations with the data

After the brief description of the theoretical models, we proceed with a comparison of their predictions with our data. Comparing first the DIT calculations with the 15 MeV/nucleon data (Figs. 6b and 7b), we see that the DIT results on the Δ–TKEL correlation show a monotonic increase similar to the experimental one, but displaced to lower values of TKEL, that is, occurring at shorter interaction times (see Fig. 5), relative to the data. On the other hand, the CoMD calculations seem to describe the 15 MeV/nucleon data in a satisfactory way for both systems ^{86}Kr+^{64,58}Ni and ^{86}Kr+^{124,112}Sn. Our interpretation of this observation goes as follows. It has been shown that CoMD (as well as other codes, e.g. BNV, BUU, TDHF) predicts the development of a collective behavior during the interaction of the projectile with the target in a peripheral or semi-peripheral collision [59, 60]. A certain time is necessary for a neck to develop between the projectile and the target after their contact. During this initial stage, a giant dipole oscillation of the neutrons against the protons in the deformed dinuclear complex develops that retards the net transfer of isospin between the two isospin asymmetric nuclei. Consequently, a retardation of the process of net N/Z transport during the interaction between the asymmetric nuclei is to be expected. This retardation due to the collective response of the two nuclei in contact is a purely mean-field effect and it is not present in the calculations of the DIT model which assumes a prompt initiation of stochastic exchange of nucleons.

The present 15 MeV/nucleon data support such an interpretation: for the ^{86}Kr+Ni system, the Δ values start to change appreciably after a TKEL of $\approx$50 MeV ($t_{int} \approx$ 40 fm/c, using the CoMD calculations of Fig. 5), whereas for the ^{86}Kr+Sn system, after a TKEL of $\approx$100 MeV ($t_{int} \approx$ 60 fm/c). Thus a retardation of the process of N/Z equilibration is clearly seen in the data and the CoMD calculations for the 15 MeV/nucleon systems.

For the 25 MeV/nucleon Kr+Sn system (Fig. 8b), the retardation of the N/Z transport is not present in the Δ–TKEL data. This is in agreement with the observed suppression of the collective dynamical-dipole response at this energy according to the studies in [61]. For the 25 MeV/nucleon system, we see that the DIT calculations of N/Z (Fig. 8a) promptly depart from the projectile value and go toward the N/Z equilibrium values with increasing TKEL. The Δ values (Fig. 8b) appear to follow the data for the first 1/3 of the TKEL range. We suspect that the disagreement of the calculation with the data at the higher part of the TKEL may in part be due to an incomplete reconstruction of TKEL for the corresponding highly dissipative events (see Figs. 4c, 4d and relevant discussion in Section III-B). For the CoMD calculations, the N/Z values are lower than the corresponding

ones from DIT for the following reason: for the reaction at 25 MeV/nucleon an increased neutron emission is expected to occur between the end of the projectile–target interaction and the time t=300 fm/c when the CoMD calculations were stopped. This neutron emission is, of course, expected to be more pronounced for the neutron rich ^{86}Kr+^{124}Sn system compared to the less neutron-rich ^{86}Kr+^{112}Sn system. (The corresponding average number of neutrons are 1.3 and 0.8 for the neutron-rich and the neutron-deficient quasiprojectiles, respectively, in approximately the middle of the TKEL range as seen in Fig. 8a). Thus, the resulting Δ–TKEL correlation departs from the corresponding ones of DIT and the data.

Moreover, it is interesting to note that both the asy-stiff and the asy-soft symmetry potentials employed in CoMD give similar results as seen in Figs. 6, 7 and 8 (compare the full and dotted lines). This observation implies that the average Δ – TKEL correlation is rather insensitive to the variation of the symmetry potential with density (as implemented in CoMD) in the range of densities involved in peripheral and semiperipheral collisions at the present energies of 15–25 MeV/nucleon. We will present a semi-quantitative interpretation in subsection C.

B. Additional isoscaling data and model comparisons

For reasons of completeness of the present study, in this section we present the isoscaling analysis of heavy residue data from the interaction of a ^{64}Ni projectile at 25 MeV/nucleon with ^{64,58}Ni and ^{124,112}Sn targets. These heavy-residue data [65] were obtained with the BigSol separator in the forward angular range of $\Delta\theta = 1.5^o$–2.5^o, which lies well inside the grazing angle for both reactions ^{64}Ni+Ni ($\theta_{gr} \approx 4.0^o$) and ^{64}Ni+Sn ($\theta_{gr} \approx 6.5^o$). This experimental condition resulted in the inability to collect projectile fragments produced in very peripheral collisions, in contrast to the ^{86}Kr(25MeV/nucleon)+Sn study already presented.

Following the analysis procedures laid out in this work, we show in Fig. 9a the variation of the isoscaling parameter α with respect to Z for ^{64}Ni+^{64,58}Ni (open points) and ^{64}Ni+^{124,112}Sn (closed points). In Figs 9b, 9c and 9d, we show respectively, the average velocities, the resulting TKEL and the quasiprojectile E*/A with respect to Z. We see that, due to the kinematical selection mentioned above, fragments near the projectile (Z=27,28) are observed to have velocities substantially lower than that of the beam; thus, they correspond to collisions with larger TKEL and quasiprojectiles substantially more excited, as compared to the corresponding near-projectile fragments observed in the ^{86}Kr(25MeV/nucleon)+Sn reactions, shown in the corresponding Figs. 4b, 4c and 4d. In Fig. 10b, the experimental Δ–TKEL correlations are shown for the ^{64}Ni+^{64,58}Ni systems. The absence of low TKEL points with corresponding low values of Δ is apparent. The DIT calculations seem to describe the data rather adequately, whereas the CoMD results are at lower values of Δ for given TKEL. Looking at Fig. 10a, as expected for the isospin symmetric ^{64}Ni+^{64}Ni system, the DIT prediction follows the horizontal N/Z line for ^{64}Ni, whereas the CoMD calculation follows a line displaced to lower N/Z values due to pre-equilibrium neutron emission. (The CoMD line corresponds to the emission of ∼0.6 neutrons from a Ni-like quasiprojectile in the middle of the TKEL range). For the isospin asymmetric system ^{64}Ni+^{58}Ni, both the DIT and the CoMD follow a monotonic variation toward full N/Z equilibrium, with the CoMD being mostly lower than DIT after a TKEL of ∼ 100 MeV.

For the ^{64}Ni+^{124,112}Sn systems, the data shown in Fig. 11b, start already at highly dissipative events (TKEL ∼300 MeV) and tend toward N/Z equilibrium. The DIT calculations of N/Z (Fig. 11a) for the neutron-rich system ^{64}Ni+^{124}Sn moves toward N/Z equilibrium with TKEL. However, for the neutron-deficient system ^{64}Ni+^{112}Sn they cross the N/Z equilibrium line and move beyond, driven by the slope of the potential energy surface of this dinuclear system that involves the rather proton-rich ^{112}Sn target. The comparison of the DIT calculations with the data (Fig. 11b) is not especially satisfactory, being rather similar to that shown in Fig. 8b for ^{86}Kr(25MeV/nucleon)+^{124,112}Sn above a TKEL of ∼400 MeV. Again, we may attribute this discrepancy to a possible incomplete reconstruction of the TKEL for the involved highly dissipative events. Concerning the CoMD calculations (Fig. 11a), the N/Z lines lie below the corresponding DIT lines (due to neutrom emission, as discussed above) and their difference (Fig. 11b) lies below the corresponding DIT line, with some similarity to the corresponding line in Fig. 8b. Closing the presentation of the 25 MeV/nucleon data on ^{64}Ni+^{64,58}Ni and ^{64}Ni+^{124,112}Sn, we note the incomplete character of these residue data obtained rather far inside the grazing angles for the corresponding systems. However, their analysis shows consistency compared to the already presented complete data set of 25 MeV/nucleon ^{86}Kr+^{124,112}Sn, which, we remind was studied at and near the corresponding grazing angle [64].

Finally we present the isoscaling data of the ligher system ^{40}Ar+^{64,58}Ni at 15 MeV/nucleon. These data were obtained with the MARS recoil separator with an experimental setup similar to that of the 15 MeV/nucleon ^{86}Kr+^{64,58}Ni,^{124,112}Sn data, in efforts to measure the production rates of rare neutron-rich isotopes near sulfur [66]. The measurements were performed in the angular range of $\Delta\theta = 2.2^o$–5.8^o, well suited for near-projectile fragments from the above reaction with ($\theta_{gr} \approx 7.0^o$).

The isoscaling data for the observed heavy projectile fragments are shown in Fig. 12a. In Fig. 12b, the variation of the isoscaling parameter α with respect to Z is given. (The value for Z=18 is missing, since we could not obtain an isoscaling line for Ar, due to the presence of elastic scattering). For this light projectile, we

observe an increasing value of α as we move from near-projectile fragments (and thus very peripheral collisions) to fragments further from the projectile (coming from more dissipative events). Following the analysis strategy of this work, we show respectively, in Figs 13a, 13b and 13c, the average velocities, the resulting TKEL and the quasiprojectile E*/A with respect to Z. Finally, in Fig. 14b, we present the experimental data on the Δ–TKEL correlation. For this lighter system at 15 MeV/nucleon, we see again the evolution of the process of N/Z equilibration with respect to TKEL. However, we do not see a retardation of the process as that observed at 15 MeV/nucleon for the heavier systems ^{86}Kr+Ni,Sn. The DIT calculations (absolute values of N/Z in Fig. 14a and differences in Fig. 14b) follow the data rather well except at the higher points. The CoMD calculations of N/Z show some displacement with respect to N/Z for the neutron rich system (Fig. 14a). The CoMD calculated differences Δ also show some displacement compared to the DIT and the data (Fig. 14b). However they do not show any retardation as that observed in the ^{86}Kr+Ni,Sn systems. We may conclude that for this lighter system at 15 MeV/nucleon the collective character of the N/Z process is possibly suppressed relative to the mechanism of stochastic nucleon exchange.

C. A combined scaling of the 15 MeV/nucleon and the 25 MeV/nucleon data

In this section we attempt to combine the heavy-residue isoscaling results on the Δ – TKEL correlation for the 15 MeV/nucleon and 25 MeV/nucleon systems presented in this work. In Fig. 15 we show such a combined plot. On the horizontal axis we plot the fraction of the TKEL relative to the maximum value allowed for binary collisions for the respective systems. On the vertical axis, we show the fraction of quasiprojectile Δ relative to that of the corresponding dinuclear system (composite system) Δ_{cs} in full isospin equilibration.

Interestingly, two distinct lines of data points appear: first, the 15 MeV/nucleon data of ^{86}Kr+^{64,58}Ni (open circles) and ^{86}Kr+^{124,112}Sn (full circles); second, all the 25 MeV/nucleon data, namely, ^{86}Kr+^{124,112}Sn (full squares), ^{64}Ni+^{64,58}Ni (upright triangles) and ^{64}Ni+^{124,112}Sn (diamonds), along with the 15 MeV/nucleon data of ^{40}Ar+^{64,58}Ni (inverted triangles). The second group of data points appears to follow a straight line passing from the origin. For these systems, as already discussed in the previous section, the process of N/Z equilibration starts promptly and is consistent with the mechanism of stochastic nucleon exchange between the two interacting nuclei. A simple semi-quantitative interpretation of the observed proportionality of Δ/Δ_{cs} to TKEL/TKEL$_{max}$ may be provided using Eq. 8. The slope of the above proportionality essentially expresses the rate of diffusion of the isospin (or, exactly, of the isospin difference): Δ/Δ_{cs} designates the extent of isospin transport and TKEL/TKEL$_{max}$ is connected with the interaction time. Under the assumption of a constant spatial curvature of I, i.e. $\nabla^2 I \sim$ const., (and thus of ΔI, i.e. $\nabla^2(\Delta I) \sim$ const.), Eq. 8 and Eq. 5 indicate the dependence of the slope on the strength of $S_{sym}(\rho)$ which may be taken as nearly constant on average for densities ρ near the normal nuclear density ρ_o, as may be assumed for peripheral and semiperipheral collisions. (The same arguments may explain the insensitivity of the CoMD calculations to the choice of the symmetry potential in CoMD, as seen in Figs. 6, 7 and 8.)

On the contrary, for the first group of data involving the 15 MeV/nucleon heavy systems ^{86}Kr+^{64,58}Ni and ^{86}Kr+^{124,112}Sn, the process of N/Z equilibration is markedly retarded: net isospin transport appears to start after ∼20% of the available TKEL has been dissipated, which corresponds to events with interaction time longer than 60–80 fm/c, according to the CoMD predictions of Fig. 5 for the corresponding systems. As we already discussed, we attribute this retardation to the collective response of the isospin asymmetric projectile–target system being brought into contact. As we mentioned in Section V-A, we expect that a neck will form between the projectile and the target. A non-equilibrium collective dipole motion of the neutrons against the protons of the initially isospin-asymmetric dinuclear system will start whose amplitute will decay with time as a net transport of isospin throught the neck will take place.

As noted in the introduction, a collective behavior in isospin-asymmetric systems has already been observed experimentally in pre-equilibrium γ-ray emission. We remind that the systematic studies of this dynamical-dipole mode have shown a rise-and-fall behavior of this mode with beam energy, with a maximum beam energy in the range 10–15 MeV/nucleon. The fact that we observe the retardation at 15 MeV/nucleon for the heavy Kr+Ni,Sn systems and not in the light Ar+Ni system, may lead us to attribute this retardation to the formation of a sizable neck in the heavy system which is not the case for the lighter system. Detailed studies of the phase space topology of the neck region with the present CoMD code, (as well as with BNV/SMF and TDHF codes) may be a necessary next step to shed light to this issue and should be undertaken in the near future.

To summarize this discussion, we draw the conclusion that the observed behavior of the present experimental data at 15 MeV/nucleon for the heavy systems and their successful description provided by CoMD are suggestive of the collective response during the first stages of these isospin-asymmetric heavy–ion collisions. The increase of the energy to 25 MeV/nucleon results in a transition from the collective response to a stochastic (chaotic) response involving the random exchange of nucleons as supported by the DIT calculations. This transition is also indicated in a self-consistent way by the behavior of the corresponding CoMD calculations at 15 MeV/nucleon and 25 MeV/nucleon.

VI. DISCUSSION

As an overview of the presented experimental approach to study the process of N/Z equilibration, we note that the observed variation of the isoscaling parameter α with Z for near-projectile residues probes the variation in the N/Z of the quasiprojectiles, directly related to the course toward N/Z equilibration. Thus, the isoscaling parameter α along with the determination of TKEL, excitation energy (and temperature) was used in our analysis to study the N/Z equilibration process in collisions of isospin asymmetric massive nuclei.

One important issue related to the isoscaling parameter α (and the application of the isoscaling in general) is the effect of the de-excitation of the hot primary residues. We point out that the isoscaling relation Eq. 7 (or Eq. 9) holds strictly for the hot primary quasiprojectiles. Nonetheless, the isoscaling properties are preserved to a large extent after the de-excitation and the values of the isoscaling parameters are rather moderately affected (see e.g. [72–74]). This is mainly due to the similarity of excitation energies of the two systems being compared (the neutron-rich and the neutron-deficient) which results in a rather comparable decrease of the relative neutron content of the hot quasiprojectiles that lead to the observed fragments (on which, of course, the experimental isoscaling procedure is based).

A question related to the present analysis of the isoscaling data spanning a wide range of energy dissipation is why non-equilibrium in the N/Z degree of freedom at the separation stage is assumed to be consistent with an equilibrium statistical description. We point out that the degree of N/Z equilibration at the separation stage is determined by the impact parameter of the collision and the ensuing interaction time. An equilibrium statistical description is applied to the hot quasiprojectile under the usual assumption that enough time has elapsed after the separation so that it is nearly at thermodynamic equilibrium.

Furthermore, we wish to provide some comments on the shape of the correlation of R_{21}(N,Z) with respect to N for given Z, especially for Z's near the projectile, as seen in Figs. 1a and 1b. A close examination reveals undulations of R_{21} as a function of N. These variations may be due, in part, to the fact that for a given Z, isotopes from a broad range of E*/A are produced whose yield ratios are presented in the figures. In an exclusive type of experiment where TKEL and E* could be obtained via kinematical reconstruction on an event-by-event basis, these variations could be explored in a finer detail. In the present approach, for a given Z, we assumed a simple exponential relation R_{21}(N,Z)–N and an average behavior with respect to dissipation to obtain an average TKEL and an average quasiprojectile E*/A, as discussed in Section III-B. Another effect that may contribute to the undulatory shape of the near-projectile isoscaling lines is the collective character of the N/Z transport in the dinuclear system. It is interesting to note the marked undulatory shape of the isoscaling lines for near-projectile Z's for the 15 MeV/nucleon ^{86}Kr+^{64,58}Ni, ^{124,112}Sn systems (Fig. 1a, 1b) and the rather smooth behavior of the corresponding isoscaling lines for the 25 MeV/nucleon ^{86}Kr+^{124,112}Sn system (Fig. 2a of [64]). Detailed microscopic calculations may help to further understand these observations.

From an experimental point of view, comparing the heavy-residue isoscaling approach with the pre-equilibrium γ-ray approach, we note that the present method offers the possibility of providing information on the evolution of the N/Z response with respect to dissipation (TKEL), following the impact parameter range from very peripheral to semiperipheral collisions. In a next generation experimental set-up, a combination of a high-resolution magnetic spectrometer with a large acceptance γ-ray (and/or light-particle) array in the target chamber will allow studies of the evolution of the collective N/Z response in isospin-asymmetric heavy–ion collisions. A systematic study of the transitional behavior of the N/Z degree of freedom with respect to beam energy and system size would be an interesting next step employing the large variety of beams available from low-energy stable-beam facilities. Of course, such studies can be extended to more isospin-asymmetric systems with the use of rare isotope beams in the near future.

Furthermore, we remind that the isovector collective response in the early stages of the reaction is responsible for the emission of pre-equilibrium γ-rays in the energy range 10–15 MeV. This emission mechanism has been proposed [61] as a cooling route for the production of superheavy elements in N/Z asymmetic fusion reactions. Along this line, we wish to suggest that the same cooling mechanism may be exploited in the production of extremely neutron-rich rare isotopes in peripheral collisions in the energy range of 15 MeV/nucleon involving neutron-rich rare isotope beams ([67, 99–101].

On the theoretical side, we wish to comment on the observation that the CoMD results on the average (N/Z) – TKEL and Δ – TKEL correlations are insensitive to the variation of the symmetry potential with density given by the two forms used in CoMD, as described in Section III-D. We point out that both of these forms (see Eq. 2 and Fig. 11 of [96]) correspond to a rather asystiff class of Skyrme functionals. It would be interesting to explore a soft symmetry potential in CoMD that bends to lower values above the saturation density, as used in BNV/SMF calculations (see Fig. 1 of [51]). It would also be of interest to examine the behavior of the CoMD calculations with respect to the absolute value of the symmetry potential at saturation density. Along this line, we may propose to explore the sensitivity of the CoMD calculations with respect to the in-medium nucleon-nucleon cross sections employed and understand their role in the transition from the collective N/Z response to the stochastic nucleon-exchange mechanism with increasing energy.

VII. SUMMARY AND CONCLUSIONS

In summary, the isoscaling of heavy projectile residues from a series of peripheral heavy-ion reactions at 15–25 MeV/nucleon is employed to obtain information on the process of N/Z equilibration with respect to energy dissipation. Recent high-resolution data from the reactions of ^{86}Kr (15 MeV/nucleon) with ^{64,58}Ni and ^{124,112}Sn were first analyzed. The yield ratios R_{21}(N,Z) of the fragments from each pair of systems exhibit isoscaling with the isoscaling parameter α increasing with decreasing (or increasing) Z away from the projectile. This variation was connected to the evolution toward N/Z equilibration with increasing energy dissipation, that was estimated from the residue velocities assuming binary kinematics. Furthermore, our previous projectile residue data at 25 MeV/nucleon for the reactions ^{86}Kr+^{124,112}Sn and ^{64}Ni+^{64,58}Ni, ^{64}Ni+^{124,112}Sn, as well as data at 15 MeV/nucleon for ^{40}Ar+^{64,58}Ni were analyzed in a similar way. Calculations with the DIT (Deep-Inelastic Transfer) model and the CoMD (Constrained Molecular Dynamics) model provided an overall satisfactory description of the experimental observables of the present analysis and gave guidance for the interpretation of the results. The isoscaling data of the ^{86}Kr+Ni,Sn reactions at 15 MeV/nucleon show a retardation of the process of N/Z equilibration which, following the CoMD calculations, is suggestive of a collective character of the process, possibly related to a sizable neck formation. This retardation is not present in the investigated systems at 25 MeV/nucleon (and the light ^{40}Ar+Ni systems at 15 MeV/nucleon), which behave in a way consistent with stochastic nucleon exchange, as inferred by their agreement with the predictions of the DIT model. No sensitivity of the N/Z observable was found to the density dependence of the symmetry potential employed in the CoMD code, providing nearly similar results with a stiff as well as a soft density-dependent symmetry potential. The present isoscaling analysis based on high-resolution mass spectrometric data of heavy residues offers a detailed description of the process of N/Z equilibration and can be extended to more asymmetric systems using rare isotope beams. This approach provides important information on the mechamism of isospin equilibration in peripheral collisions, complementary to that accessible from modern large-acceptance (γ-ray and/or light-particle) multidetector devices and, in conjunction with the latter, may shed light to the degree of collectivity of nuclear matter as a function of energy. Moreover, it may serve as a rigorous testing ground of modern microscopic models of heavy-ion collisions.

VIII. ACKOWLEDGEMENTS

We are thankful to L. Tassan-Got for the DIT code, to M. Papa for his version of the CoMD code and to Hua Zheng for his rewritten version of the CoMD code and useful discussions. Furthermore, we acknowledge the motivation and recent discussions with Y.K. Kwon and K. Tshoo of the KOBRA team of RISP. Financial support for this work was provided, in part, by ELKE Research Account No 70/4/11395 of the National and Kapodistrian University of Athens, and by the U.S. Department of Energy under Grant No. DE-FG03-93ER40773 and by the Robert A. Welch Foundation under Grant No. A-1266. M.V. was supported by the Slovak Scientific Grant Agency under contracts 2/0105/11 and 2/0121/14 and by the Slovak Research and Development Agency under contract APVV-0177-11.

[1] T. Baumann, A. Spyrou, and M. Thoennessen, Rep. Prog. Phys. **75**, 036301 (2012).
[2] J. Erler, N. Birge, M. Kortelainen, W. Nazarewicz, et al., Nature **486**, 509 (2012).
[3] J. Äystö, W. Nazarewicz, M. Pfützner, and C. Signorini, eds., *Proceedings of the Fifth International Conference on Exotic Nuclei and Atomic Masses (ENAM'08), Ryn, Poland, September 7–13 (2008)* (Eur. Phys. J. A, 42, 2009).
[4] M. Thoennessen and B. M. Sherrill, Nature **473**, 25 (2011).
[5] C. Sneden and J. J. Cowan, Science **299**, 70 (2003).
[6] K. Langanke and M. Wiescher, Rep. Prog. Phys. **64**, 1657 (2001).
[7] H.-T. Janka, K. Langanke, A. Marek, G. Martínez-Pinedo, and B. Müller, Phys. Rep. **442**, 38 (2007).
[8] P. Danielewicz, R. Lacey, and W. G. Lynch, Science **298**, 1592 (2002).
[9] B.-A. Li, L. W. Chen, and C. M. Ko, Phys. Rep. **464**, 113 (2008).
[10] D. V. Shetty, S. J. Yennello, and G. A. Souliotis, Phys. Rev. C **76**, 024606 (2007).
[11] V. Baran et al., Phys. Rep. **410**, 335 (2005).
[12] G. Giuliani, H. Zheng, and A. Bonasera, Prog. Part. Nucl. Phys. **76**, 116 (2014).
[13] Z. Kohley and S. J. Yennello, Eur. Phys. J. A **50**, 31 (2013).
[14] A. R. Raduta and F. Gulminelli, Phys. Rev. C **82**, 065801 (2010).
[15] A. S. Botvina and I. N. Mishustin, Nucl. Phys. A **843**, 98 (2010).
[16] N. Buyukcizmeci, A. Botvina, I. Mishustin, et al., Nucl. Phys. A **907**, 13 (2013).
[17] C. J. Pethick and D. G. Ravenhall, Ann. Rev. Nucl. Part. Sci. **45**, 429 (1995).
[18] J. M. Lattimer and M. Prakash, Phys. Rep. **442**, 109 (2007).
[19] E. O. Connor and C. D. Ott, Class. Quantum Grav. **27**, 114103 (2010).
[20] M. D. Toro, V. Baran, M. Colonna, et al., Prog. Part. Nucl. Phys. **62**, 389 (2009).
[21] B.-A. Li and W. Schroeder, eds., *Isospin Physics in*

Heavy Ion Collisions at Intermediate Energies (Nova Science, New York, 2001).
[22] V. V. Volkov, Phys. Rep. **44**, 93 (1978).
[23] W. U. Schoeder and J. R. Huizenga, *Treatise on Heavy-Ion Science, Vol. 2, Chapter 3* (Plenum, New York, 1984).
[24] H. Freiesleben and J. V. Kratz, Phys. Rep. **106**, 1 (1984).
[25] M. Petrovici et al., Nucl. Phys. A **477**, 277 (1988).
[26] R. Planeta et al., Phys. Rev. C **38**, 195 (1988).
[27] R. T. deSouza et al., Phys. Rev. C **39**, 114 (1989).
[28] R. T. deSouza et al., Phys. Rev. C **37**, 1901 (1988).
[29] R. T. deSouza et al., Phys. Rev. C **37**, 1783 (1988).
[30] S. J. Yennello et al., Phys. Lett. B **321**, 15 (1994).
[31] B.-A. Li and S. J. Yennello, Phys. Rev. C **52**, 1746 (1995).
[32] H. Johnston et al., Phys. Lett. B **371**, 186 (1996).
[33] I. Lombardo et al., Phys. Rev. C **82**, 014608 (2010).
[34] M. B. Tsang et al., Phys. Rev. Lett. **92**, 062701 (2004).
[35] G. Ademard, B. Borderie, A. Chbihi, et al., Eur. Phys. J. A **50**, 33 (2014).
[36] M. Veselsky et al., Phys. Rev. C **62**, 064613 (2000).
[37] A. L. Keksis et al., Phys. Rev. C **81**, 054602 (2010).
[38] S. Barlini, S. Piantelli, G. Casini, et al., Phys. Rev. C **87**, 054607 (2013).
[39] E. D. Filippo, A. Pagano, P. Russotto, et al., Phys. Rev. C **86**, 014610 (2012).
[40] Z. Kohley et al., Phys. Rev. C **83**, 044601 (2011).
[41] J. Rizzo, M. Colonna, V. Baran, et al., Nucl. Phys. A **806**, 79 (2008).
[42] D. Thériault, J. Gauthier, F. Grenier, et al., Phys. Rev. C **74**, 051602 (2006).
[43] K. Brown, S. Hudan, R. T. deSouza, et al., Phys. Rev. C **87**, 061601 (2013).
[44] S. Hudan, A. B. McIntosh, R. T. deSouza, et al., Phys. Rev. C **86**, 021603 (2012).
[45] J. Randrup, Nucl. Phys. A **307**, 319 (1978).
[46] J. Randrup, Nucl. Phys. A **327**, 490 (1979).
[47] L. Tassan-Got and C. Stefan, Nucl. Phys. A **524**, 121 (1991).
[48] B.-A. Li, C. B. Das, S. D. Gupta, and C. Gale, Nucl. Phys. A **735**, 563 (2004).
[49] L. W. Chen, C. M. Ko, and B.-A. Li, Phys. Rev. Lett. **94**, 032701 (2005).
[50] V. Baran, M. Colonna, M. D. Toro, M. Zielinska-Pfabé, and H. H. Wolter, Phys. Rev. C **72**, 064620 (2005).
[51] C. Rizzo, V. Baran, M. Colonna, A. Corsi, and M. D. Toro, Phys. Rev. C **83**, 014604 (2011).
[52] K. Sekizawa and K. Yabana, Phys. Rev. C **88**, 014614 (2013).
[53] B. Yilmaz, S. Ayik, D. Lacroix, and K. Washiyama, Phys. Rev. C **83**, 064615 (2011).
[54] Y. Iwata, T. Otsuka, J. A. Maruhn, and N. Itagaki, Phys. Rev. Lett. **104**, 252501 (2010).
[55] J. Aichelin, Phys. Rep. **202**, 233 (1991).
[56] M. Papa et al., Phys. Rev. C **64**, 024612 (2001).
[57] M. Papa et al., J. Comp. Phys. **208**, 403 (2005).
[58] V. Baran, C. Rizzo, M. Colonna, M. D. Toro, and D. Pierroutsakou, Phys. Rev. C **79**, 021603 (2009).
[59] M. Papa, W. Tian, G. Giuliani, et al., Phys. Rev. C **72**, 064608 (2005).
[60] M. Papa, A. Bonanno, F. Amorini, et al., Phys. Rev. C **68**, 034606 (2003).
[61] D. Pierroutsakou, B. Martin, C. Agodi, et al., Phys. Rev. C **80**, 024612 (2009).
[62] D. Pierroutsakou, B. Martin, G. Inglima, et al., Phys. Rev. C **71**, 054605 (2005).
[63] H. Fuchs and K. Möhring, Rep. Prog. Phys. **57**, 231 (1994).
[64] G. A. Souliotis, M. Veselsky, D. V. Shetty, and S. J. Yennello, Phys. Lett. B **588**, 35 (2004).
[65] G. A. Souliotis et al., Phys. Rev. C **73**, 024606 (2006).
[66] G. A. Souliotis et al., Progress in Research, Cyclotron Institute, Texas A&M University (2008–2009), p. II-25; accessible at: http://cyclotron.tamu.edu/publications.html (2009).
[67] G. A. Souliotis et al., Phys. Rev. C **84**, 064607 (2011).
[68] R. E. Tribble, R. H. Burch, and C. A. Gagliardi, Nucl. Instr. and Meth. A **285**, 441 (1989).
[69] W. W. Wilcke et al., At. Data Nucl. Data Tables **25**, 389 (1980).
[70] G. A. Souliotis et al., Phys. Lett. B **543**, 163 (2002).
[71] G. A. Souliotis et al., Nucl. Phys. A **705**, 279 (2002).
[72] M. B. Tsang et al., Phys. Rev. Lett. **86**, 5023 (2001).
[73] M. B. Tsang et al., Phys. Rev. C **64**, 054615 (2001).
[74] A. S. Botvina, O. V. Lozhkin, and W. Trautmann, Phys. Rev. C **65**, 044610 (2002).
[75] G. A. Souliotis et al., Phys. Rev. C **68**, 024605 (2003).
[76] G. A. Souliotis et al., Nucl. Phys. A **746**, 526 (2004).
[77] M. Veselsky, G. Souliotis, and M. Jandel, Phys. Rev. C **69**, 044607 (2004).
[78] M. Colonna and M. B. Tsang, Eur. Phys. J. A **30**, 165 (2006).
[79] M. Veselsky, Nucl. Phys. A **705**, 193 (2002).
[80] J. F. LeColley et al., Phys. Lett. B **325**, 317 (1994).
[81] M. Morjean et al., Nucl. Phys. A **591**, 371 (1995).
[82] P. Moller, J. R. Nix, and K. L. Kratz, At. Data Nucl. Data Tables **66**, 131 (1997).
[83] H. Madani et al., Phys. Rev. C **54**, 1291 (1996).
[84] J. Tõke and W. U. Schroeder, Annu. Rev. Nucl. Part. Sci. **42**, 401 (1992).
[85] S. Shlomo and V. M. Kolomietz, Rep. Prog. Phys. **68**, 1 (2005).
[86] J. B. Natowitz et al., Phys. Rev. C **65**, 034618 (2002).
[87] G. Chaudhuri, S. D. Gupta, and M. Mocko, Nucl. Phys. A **813**, 293 (2008).
[88] S. Galanopoulos et al., Nucl. Phys. A **837**, 145 (2010).
[89] S. Wuenschel et al., Phys. Rev. C **79**, 061602 (2009).
[90] P. Marini et al., Phys. Rev. C **85**, 034617 (2012).
[91] P. Marini et al., Nucl. Instrum. and Methods in Phys. Res. A **707**, 80 (2013).
[92] L. Tassan-Got, PhD Thesis, University of Caen (1989).
[93] M. Veselsky et al., Nucl. Phys. A **724**, 431 (2003).
[94] M. Veselsky and G. A. Souliotis, Nucl. Phys. A **765**, 252 (2006).
[95] M. Veselsky and G. A. Souliotis, Nucl. Phys. A **872**, 1 (2011).
[96] M. Papa, Phys. Rev. C **87**, 014001 (2013).
[97] G. Casini et al., Eur. Phys. J. A **9**, 491 (2000).
[98] G. Fabbri, M. Colonna, and M. D. Toro, Phys. Rev. C **58**, 3508 (1998).
[99] K. Tshoo, Y. K. Kim, Y. K. Kwon, et al., Nucl. Instrum. Methods Phys. Res. B **317**, 242 (2013).
[100] Y. K. Kwon and K. Tshoo, private communication.
[101] P. N. Fountas, G. A. Souliotis, M. Veselsky, and A. Bonasera, Phys. Rev. C, submitted **00**, 0000 (2014).

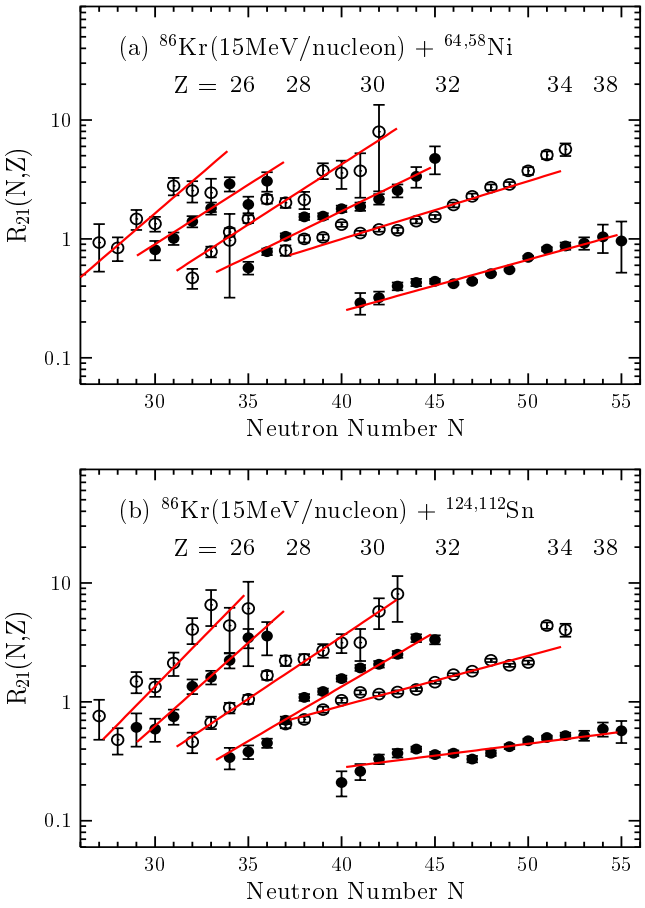

FIG. 1: (Color Online) (a) Yield ratios $R_{21}(N,Z) = Y_2(N,Z)/Y_1(N,Z)$ of projectile residues from the reactions of ^{86}Kr (15 MeV/nucleon) with ^{64,58}Ni with respect to N for the Z's indicated. (b) Yield ratios $R_{21}(N,Z) = Y_2(N,Z)/Y_1(N,Z)$ of projectile residues from the reactions of ^{86}Kr (15 MeV/nucleon) with ^{124,112}Sn with respect to N for the Z's indicated. The data are given by alternating filled and open circles, whereas the lines are exponential fits.

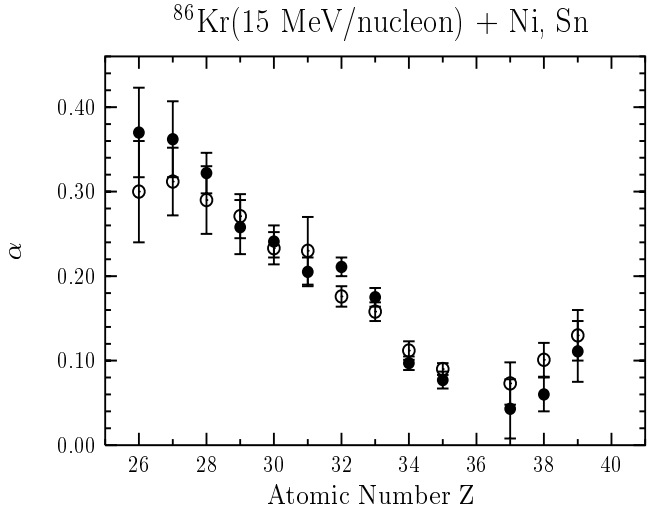

FIG. 2: Isoscaling parameter α as a function of Z for projectile residues from the reactions ^{86}Kr(15 MeV/nucleon)+^{64,58}Ni (open circles) and ^{86}Kr(15 MeV/nucleon)+^{124,112}Sn (closed circles).

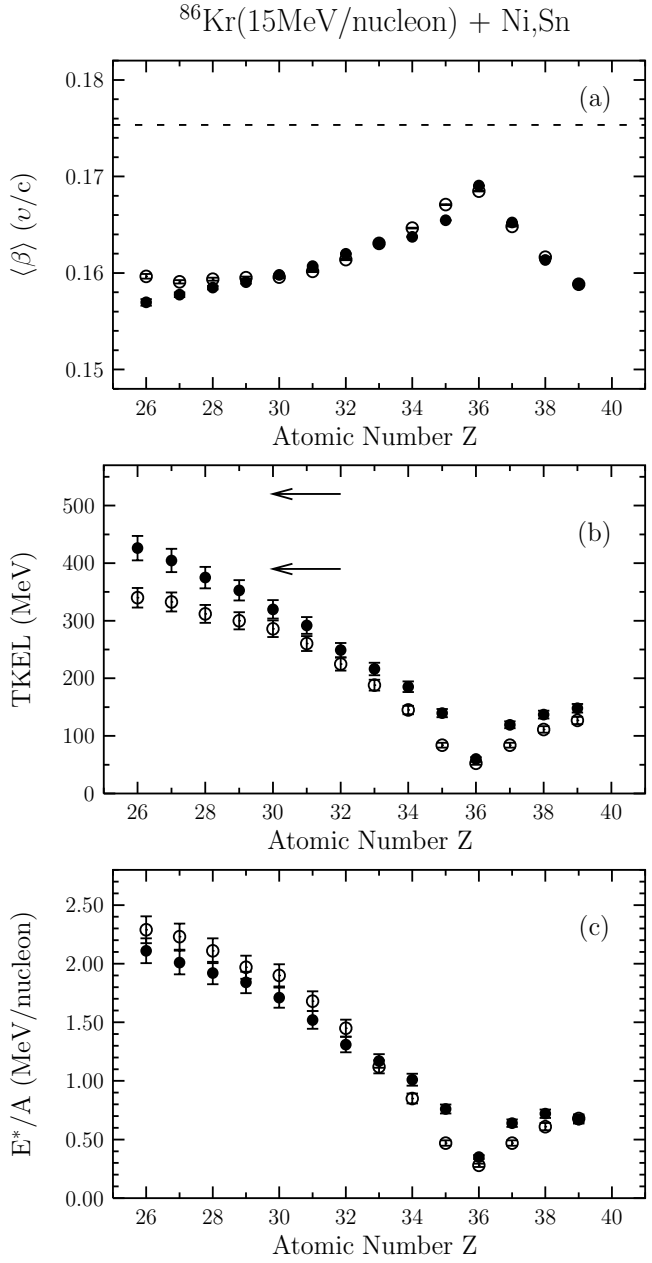

FIG. 3: (a) Average velocity versus Z correlations for projectile residues from the reactions of ^{86}Kr (15 MeV/nucleon) with ^{64}Ni (open points) and ^{124}Sn (closed points). The dashed line gives the projectile velocity. (b) Total kinetic energy loss (TKEL) vs Z evaluated from residue velocities. The arrows indicate the maximum TKEL for Kr+Ni (lower arrow) and Kr+Sn (upper arrow). (c) Excitation energy per nucleon for the quasiprojectiles vs Z evaluated from TKEL (see text).

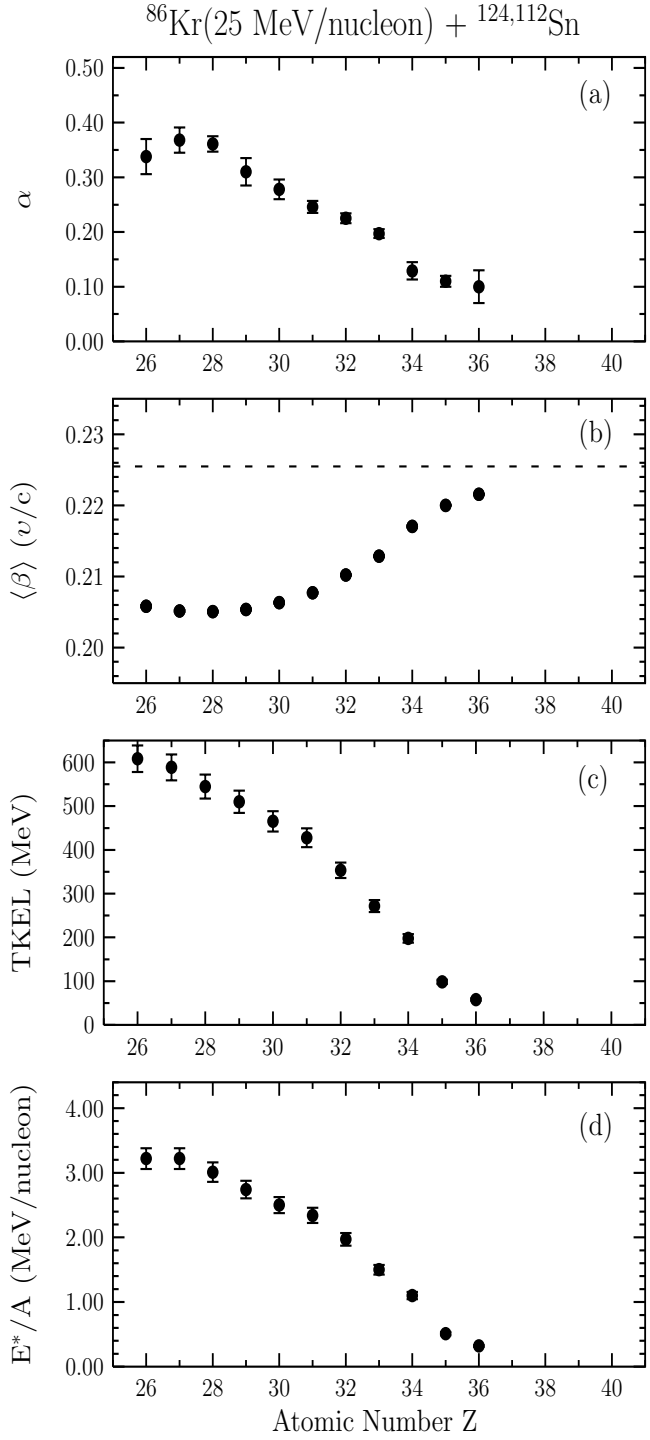

FIG. 4: (a) Isoscaling parameter α as a function of Z for projectile residues from the reactions ^{86}Kr(25 MeV/nucleon)+^{124,112}Sn [64]. (b) Average velocity versus Z correlations for projectile residues from the reaction of ^{86}Kr (25 MeV/nucleon) with ^{124}Sn. The dashed line gives the projectile velocity. (c) Total kinetic energy loss (TKEL) vs Z evaluated from residue velocities. The maximum TKEL is ∼1040 MeV (not shown). (d) Excitation energy per nucleon for the quasiprojectiles vs Z evaluated from TKEL (see text).

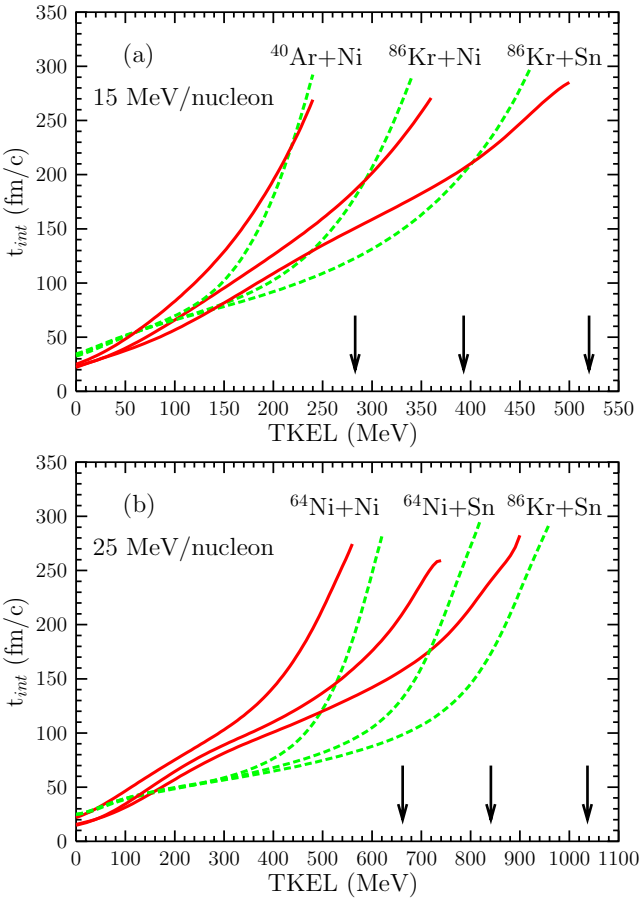

FIG. 5: (Color Online) Interaction time vs TKEL as calculated by DIT (dashed lines) and CoMD (full lines) for reactions at 15 MeV/ nucleon (a) and 25 MeV/ nucleon (b) as indicated in the figure. The arrows correspond to the maximum expected TKEL for the respective reactions.

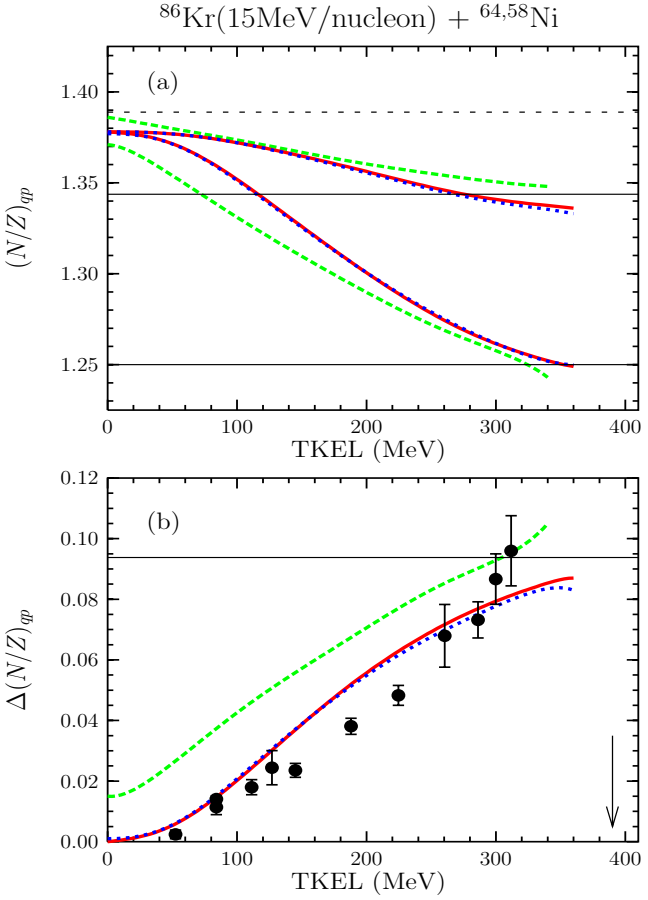

FIG. 6: (Color Online) (a) Calculated average N/Z of quasiprojectiles as a function of TKEL for the 15 MeV/nucleon reactions: ^{86}Kr+ ^{64}Ni (upper set of curves) and ^{86}Kr+ ^{58}Ni (lower set of curves). DIT calculations: dashed (green) lines. CoMD calculations: solid lines (red) for asy-stiff and dotted lines (blue) for asy-soft. Upper and lower horizontal full lines: N/Z of fully N/Z equilibrated quasiprojectiles from ^{86}Kr+ ^{64}Ni and ^{86}Kr+ ^{58}Ni reactions, respectively. Horizontal dashed line: N/Z of ^{86}Kr projectile. (b) Difference in quasiprojectile average N/Z. Lines as in (a). Points: data from the present isoscaling analysis. Horizontal full line: difference of N/Z of fully N/Z equilibrated quasiprojectiles from ^{86}Kr+ ^{64}Ni and ^{86}Kr+ ^{58}Ni reactions. Arrow: maximum TKEL of the 15 MeV/nucleon Kr+Ni reactions.

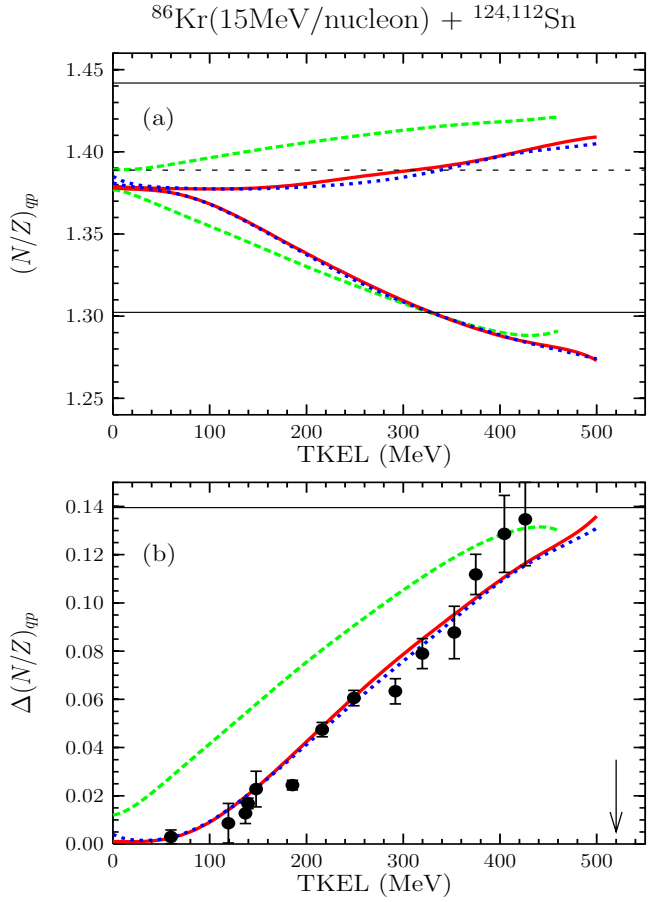

FIG. 7: (Color online) (a) Calculated average N/Z of quasiprojectiles as a function of TKEL for the 15 MeV/nucleon reactions: ^{86}Kr+ ^{124}Sn (upper set of curves) and ^{86}Kr+ ^{112}Sn (lower set of curves). DIT calculations: dashed (green) lines. CoMD calculations: solid lines (red) for asy-stiff and dotted lines (blue) for asy-soft. Upper and lower horizontal full lines: N/Z of fully N/Z equilibrated quasiprojectiles from ^{86}Kr+ ^{124}Sn and ^{86}Kr+ ^{112}Sn reactions, respectively. Horizontal dashed line: N/Z of ^{86}Kr projectile. (b) Difference in quasiprojectile average N/Z. Lines as in (a). Points: data from the present isoscaling analysis. Horizontal full line: difference of N/Z of fully N/Z equilibrated quasiprojectiles from ^{86}Kr+ ^{124}Sn and ^{86}Kr+ ^{112}Sn reactions. Arrow: maximum TKEL of the 15 MeV/nucleon Kr+Sn reactions.

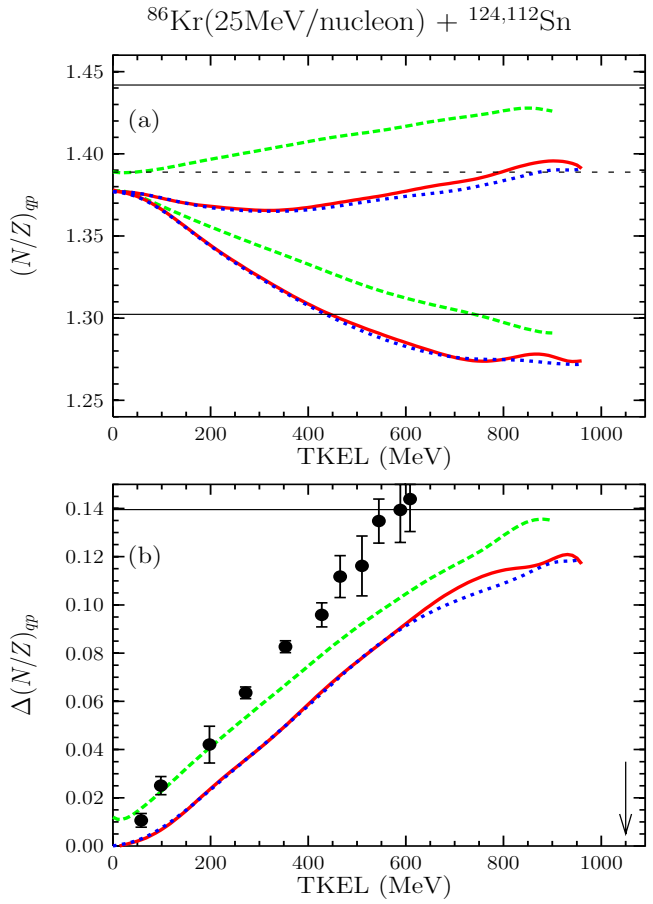

FIG. 8: (Color Online) (a) Calculated average N/Z of quasiprojectiles as a function of TKEL for the 25 MeV/nucleon reactions: ^{86}Kr+ ^{124}Sn (upper set of curves) and ^{86}Kr+ ^{112}Sn (lower set ofcurves). DIT calculations: dashed (green) lines. CoMD calculations: solid lines (red) for asy-stiff and dotted lines (blue) for asy-soft. Upper and lower horizontal full lines give the N/Z of fully N/Z equilibrated quasiprojectiles from the ^{86}Kr+ ^{124}Sn and ^{86}Kr+ ^{112}Sn reactions, respectively. Horizontal dashed line: N/Z of ^{86}Kr projectile. (b) Difference in quasiprojectile N/Z. Lines as in (a). Points: the data from the present isoscaling analysis. Horizontal full line: difference of N/Z of fully N/Z equilibrated quasiprojectiles from the ^{86}Kr+ ^{124}Sn and ^{86}Kr+ ^{112}Sn reactions. Arrow: maximum TKEL of the 25 MeV/nucleon Kr+Sn reactions.

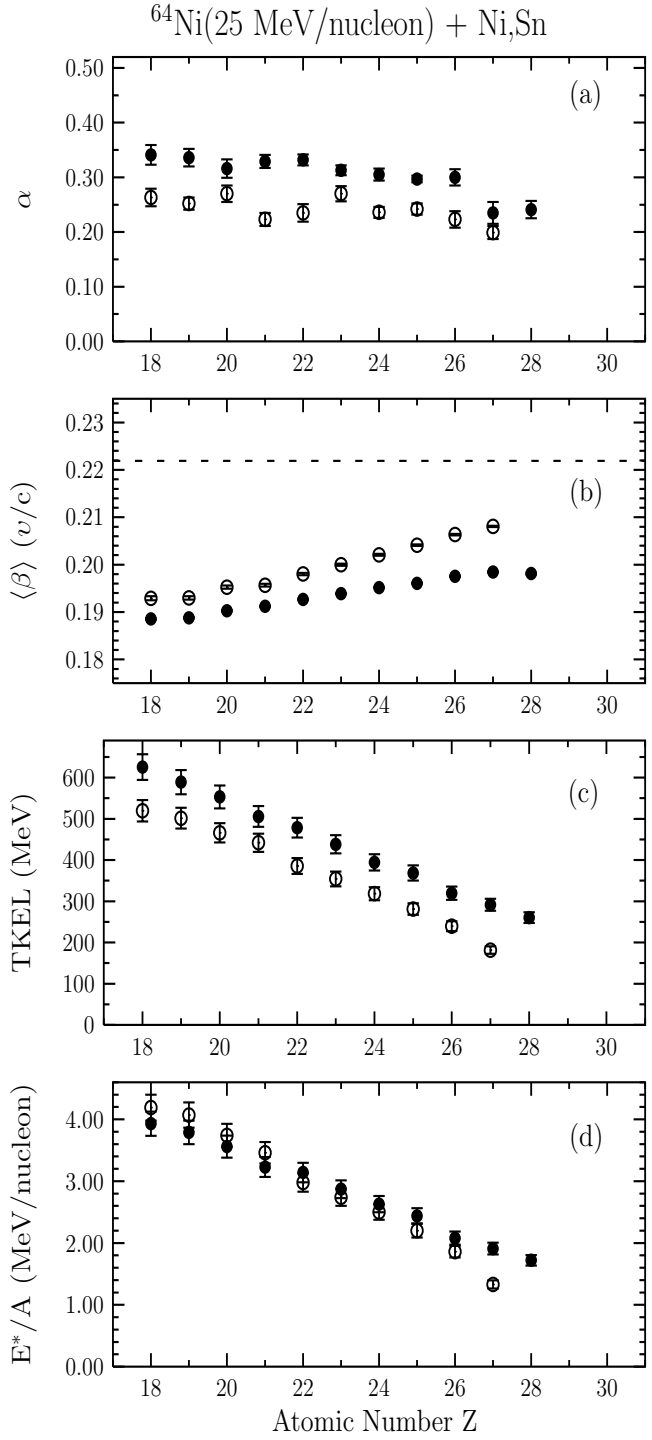

FIG. 9: (a) Isoscaling parameter α as a function of Z for projectile residues from the reactions ^{64}Ni(25 MeV/nucleon)+^{64,58}Ni (open points) and ^{64}Ni(25 MeV/nucleon)+^{124,112}Sn (closed points) [65]. (b) Average velocity versus Z correlations for projectile residues from the reactions ^{64}Ni (25 MeV/nucleon) + ^{64}Ni (open points) and ^{64}Ni (25 MeV/nucleon) + ^{124}Sn (closed points). The dashed line gives the projectile velocity. (c) Total kinetic energy loss (TKEL) vs Z evaluated from residue velocities. The symbols are as in (b). The maximum TKEL is ∼660 MeV and ∼840 MeV, respectively, for the above Ni+Ni and Ni+Sn reactions. (d) Excitation energy per nucleon for quasiprojectiles vs Z evaluated from TKEL. The points are as in (b).

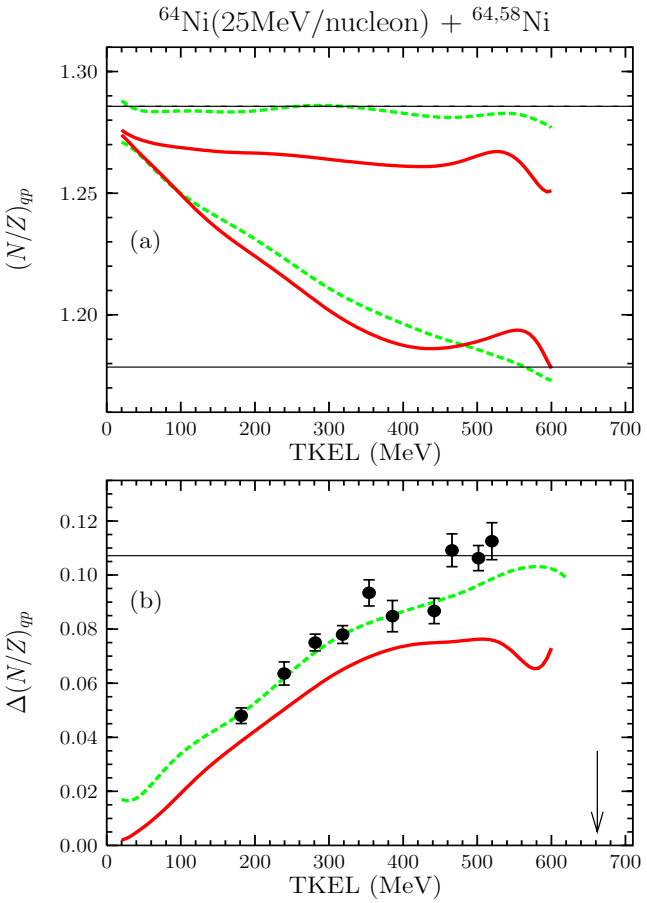

FIG. 10: (Color Online) (a) Calculated average N/Z of quasiprojectiles as a function of TKEL for the 25 MeV/nucleon reactions: ^{64}Ni + ^{64}Ni (upper set of curves) and ^{64}Ni + ^{58}Ni (lower set of curves). DIT calculations: dashed (green) lines. CoMD calculations (asy-stiff): solid (red) lines. Upper and lower horizontal full lines: N/Z of fully N/Z equilibrated quasiprojectiles from ^{64}Ni + ^{64}Ni and ^{64}Ni + ^{58}Ni reactions, respectively. The upper line, of course, coincides with the N/Z of the ^{64}Ni projectile. (b) Difference in quasiprojectile average N/Z. Lines as in (a). Points: data from the present isoscaling analysis. Horizontal full line: difference of N/Z of fully N/Z equilibrated quasiprojectiles from ^{64}Ni + ^{64}Ni and ^{64}Ni + ^{58}Ni reactions. Arrow: maximum TKEL of the 25 MeV/nucleon Ni+Ni reactions.

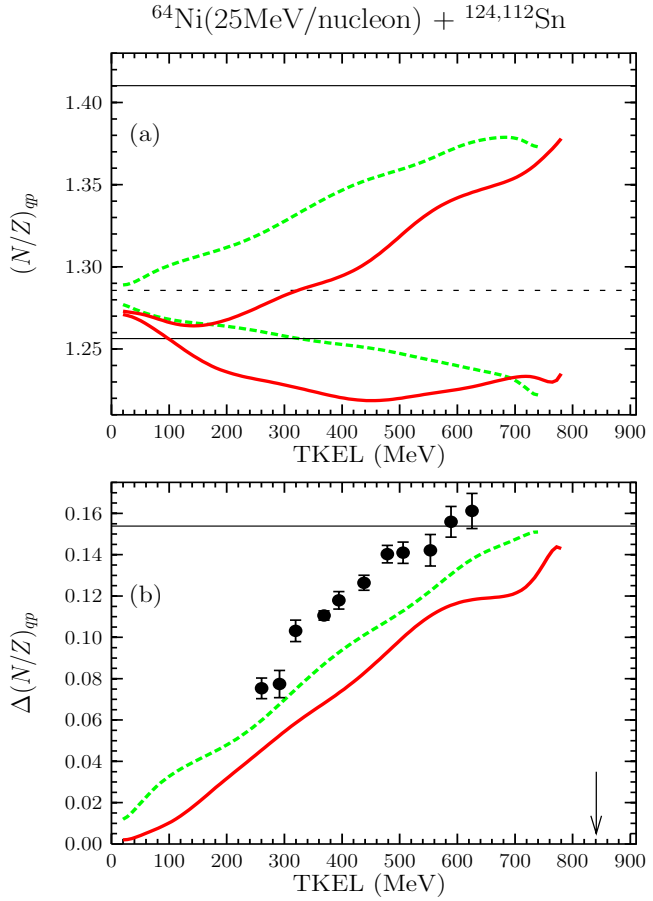

FIG. 11: (Color Online) (a) Calculated average N/Z of quasiprojectiles as a function of TKEL for the 25 MeV/nucleon reactions: ^{64}Ni + ^{124}Sn (upper set of curves) and ^{64}Ni + ^{112}Sn (lower set of curves). DIT calculations: dashed (green) lines. CoMD calculations (asy-stiff): solid (red) lines. Upper and lower horizontal full lines: N/Z of fully N/Z equilibrated quasiprojectiles from the ^{64}Ni + ^{124}Sn and ^{64}Ni + ^{112}Sn reactions, respectively. Horizontal dashed line: N/Z of ^{64}Ni projectile. (b) Difference in quasiprojectile average N/Z. Lines as in (a). Points: data from the present isoscaling analysis. Horizontal full line: difference of N/Z of fully N/Z equilibrated quasiprojectiles from the ^{64}Ni + ^{124}Sn and ^{64}Ni + ^{112}Sn reactions. Arrow: maximum TKEL of the 25 MeV/nucleon Ni+Sn reactions.

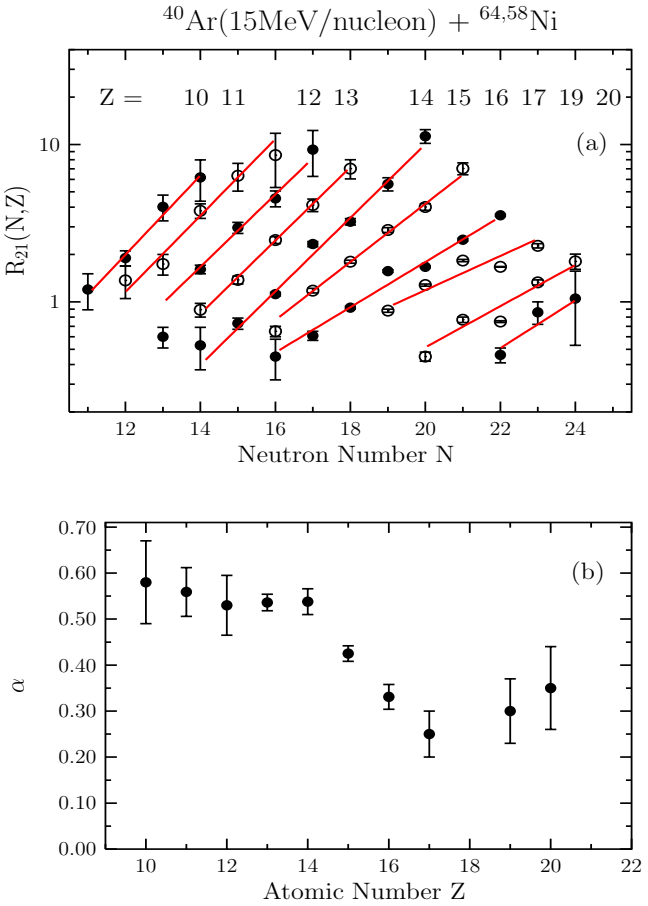

FIG. 12: (Color Online) (a) Yield ratios $R_{21}(N,Z) = Y_2(N,Z)/Y_1(N,Z)$ of projectile residues from the reactions of ^{40}Ar(15 MeV/nucleon) with ^{64,58}Ni with respect to N for the Z's indicated. The data are given by alternating filled and open circles, whereas the lines are exponential fits. (b) Isoscaling parameter α as a function of Z for projectile residues from the reactions ^{40}Ar(15 MeV/nucleon)+^{64,58}Ni.

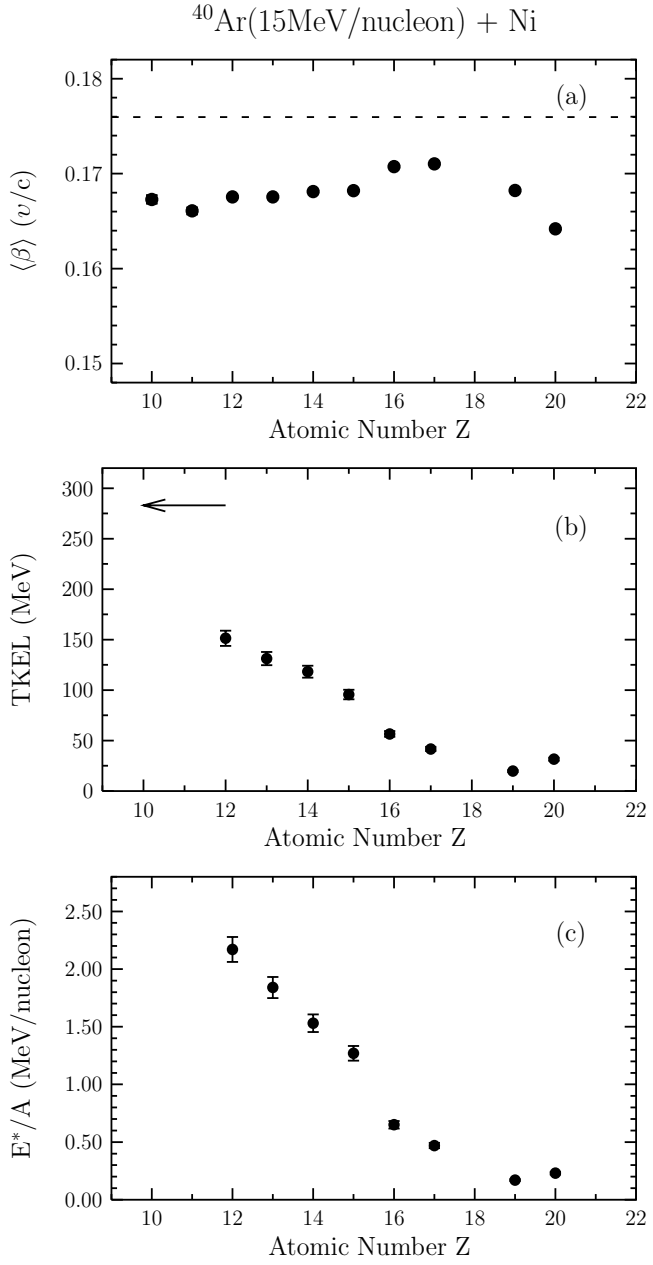

FIG. 13: (a) Average velocity versus Z correlations for projectile residues from the reaction of ^{40}Ar (15 MeV/nucleon) with ^{64}Ni. The dashed line gives the projectile velocity. (b) Total kinetic energy loss (TKEL) vs Z evaluated from residue velocities. The arrow indicates the maximum TKEL. (c) Excitation energy per nucleon for the quasiprojectiles vs Z evaluated from TKEL (see text).

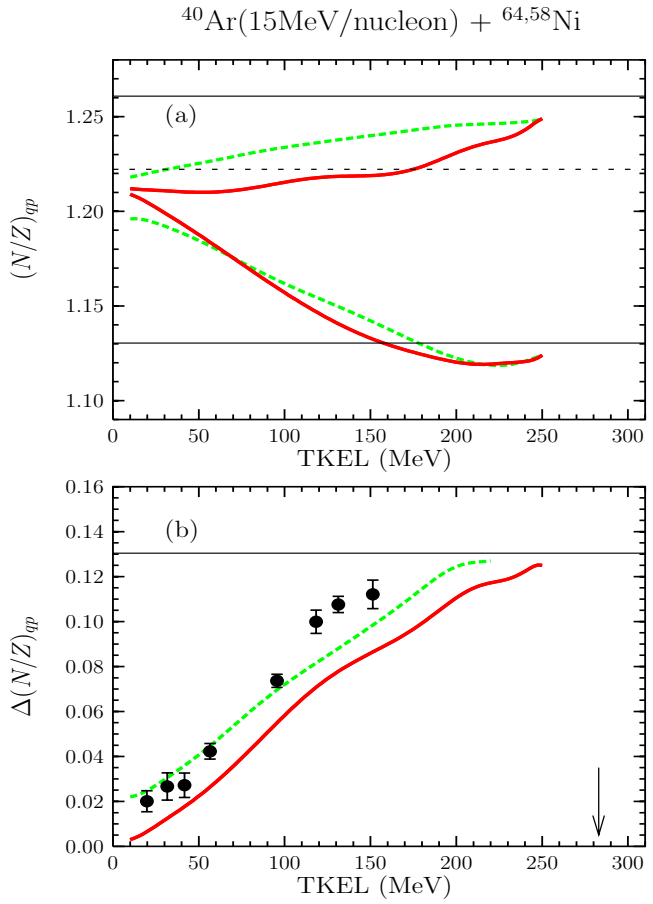

FIG. 14: (Color Online) (a) Calculated average N/Z of quasiprojectiles as a function of TKEL for the 15 MeV/nucleon reactions: ^{40}Ar + ^{64}Ni (upper set of curves) and ^{40}Ar + ^{58}Ni (lower set of curves). DIT calculations: dashed (green) lines. CoMD calculations (asy-stiff): solid (red) lines. Upper and lower horizontal full lines: N/Z of fully N/Z equilibrated quasiprojectiles from ^{40}Ar + ^{64}Ni and ^{40}Ar + ^{58}Ni reactions, respectively. Horizontal dashed line: N/Z of ^{40}Ar projectile. (b) Difference in quasiprojectile average N/Z. Lines as in (a). Points: data from the present isoscaling analysis. Horizontal full line: difference of N/Z of fully N/Z equilibrated quasiprojectiles from ^{40}Ar + ^{64}Ni and ^{40}Ar + ^{58}Ni reactions. Arrow: maximum TKEL of the 15 MeV/nucleon Ar+Ni reactions.

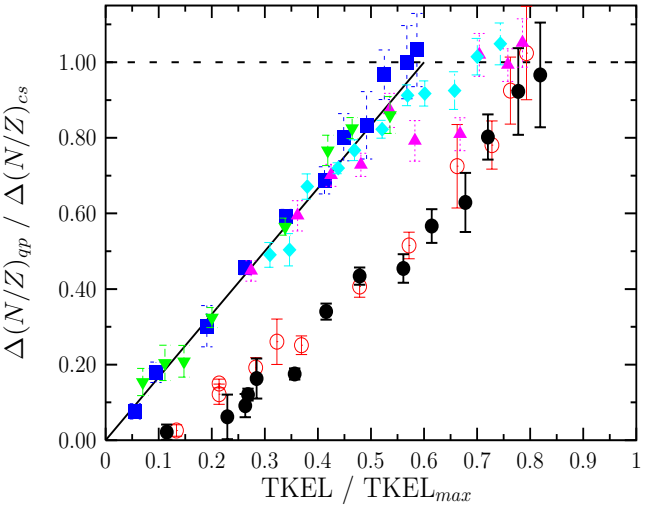

FIG. 15: (Color Online) Combined scaling of all studied systems: Horizontal axis: fraction of TKEL relative to the maximum allowed for binary collisions. Vertical axis: fraction of quasiprojectile Δ relative to that of the composite system Δ_{cs}. Open circles (red): ^{86}Kr (15 MeV/nucleon) + ^{64,58}Ni. Full circles (black): ^{86}Kr (15 MeV/nucleon) + ^{124,112}Sn. Full squares (blue): ^{86}Kr (25 MeV/nucleon) + ^{124,112}Sn. Upright triangles (magenta): ^{64}Ni (25 MeV/nucleon) + ^{64,58}Ni. Diamonds (light blue) : ^{64}Ni (25 MeV/nucleon) + ^{124,112}Sn. Inverted triangles (green): ^{40}Ar (15 MeV/nucleon) + ^{64,58}Ni. The horizontal line corresponds to full N/Z equilibration. The full line that passes from the origin gives the course of N/Z equilibration in the absence of retardation (see text).